

THROUGH-TOOL MINIMUM QUANTITY LUBRICATION AND EFFECT
ON MACHINABILITY OF INCONEL 718

A Thesis

by

WALEED ASHRAF KHAN

Submitted to the Office of Graduate and Professional Studies of
Texas A&M University
in partial fulfillment of the requirements for the degree of

MASTER OF SCIENCE

Chair of Committee,	Nguyen Hung
Co-Chair of Committee,	Li-Jung Tai
Committee Member,	Satish Bukkapatnam
Head of Department,	Andreas Polycarpou

May 2018

Major Subject: Mechanical Engineering

Copyright 2018 Waleed Ashraf Khan

ABSTRACT

This thesis simulated through-tool minimum quantity lubrication (MQL) to experimentally characterize micromist lubricant droplets. The effect of nozzle surface roughness and air pressure was analyzed to study the lubricant droplets' size, distribution and exit air velocity. MQL at different conditions was used in micromilling of Inconel 718 blocks that were additively printed by selective laser melting technique. A 3D printed nozzle simulated internal flow in commercially available drill with internal cooling channels. Anemometer was used to measure the exit air velocity of the droplets.

Droplets were collected on a glass plate from which airborne diameters and standard deviation were calculated. The droplet diameter and distribution were most sensitive when using nozzle having a rough surface with the mean airborne droplet diameter being $4.69\ \mu\text{m}$ at 550 kPa. Mean airborne droplet diameter increased to $7.60\ \mu\text{m}$ when the smooth nozzle was used at 550 kPa. Micromist generated from a rough nozzle at 550 kPa with a maximum air velocity of 13.1 m/s improved tool life by effectively lubricating the tool workpiece interface. The tool wear was reduced to approximately $41\ \mu\text{m}$ from $49\ \mu\text{m}$ measured with the use of smooth nozzle at 275 kPa. It also produced micromilled slots with surface finish S_a of $1.5\ \mu\text{m}$.

DEDICATION

This work is dedicated to my family who encouraged and helped me during my academic endeavor at Texas A&M University. Thanks for their constant support that made me go through the graduate school.

NOMENCLATURE

A	Projected area of the droplet (μm^2)
d	Diameter of the airborne droplet (μm)
D	Diameter of the internal channel of the adapter (mm)
f_d	Darcy-Weisbach friction factor (constant)
$IN718$	Inconel 718
L	Length of the internal channel of the adapter (mm)
N	Number of droplets
P	Projected diameter of the droplet (μm)
R_a	Profile Roughness (μm)
Re	Reynolds Number
S_a	Surface Roughness (μm)
U	Free stream velocity (m/s)
V'	Droplet volume (mm^3)
V	Velocity of the lubricant (m/s)
W	Width of the histogram bar
\mathcal{E}	Surface Roughness of nozzle (μm)
ρ	Density of the lubricant (Kg/m^3)
σ	Standard deviation
γ_{LG}	Interfacial tension force vector between gas and liquid (N/m)

γ_{SG}	Interfacial tension force vector between solid and gas (N/m)
γ_{SL}	Interfacial tension force vector between solid and liquid (N/m)
θ	Contact angle ($^{\circ}$)
τ	Relaxation time (s)
Δ	Distance moved by the particle towards the plate (m)
ΔP	Change in pressure (Pa)
ν	Kinematic viscosity of the lubricant (m^2/s)

CONTRIBUTORS AND FUNDING SOURCES

Contributors

I would like to thank my graduate research advisor Dr. Hung, who provided outstanding environment for conducting a research in minimum quantity lubrication and micromachining. I would also like to thank my committee members, Dr. Tai and Dr. Bukkapatnam for their guidance and support throughout my research. Special thanks to Adam Farmer for helping me with the machining experiments and metrology. I appreciate the help of Dr. King to allow me to perform experiments on Aerosol Particle Sizer in her lab.

Funding Sources

I would like to thank Unist for providing the MQL system and lubricant, Knust-Godwin for Inconel specimens, and Performance Microtools for their micromilling tools. Their support made this work possible.

TABLE OF CONTENTS

ABSTRACT	ii
DEDICATION	iii
NOMENCLATURE.....	iv
CONTRIBUTORS AND FUNDING SOURCES.....	vi
TABLE OF CONTENTS	vii
LIST OF FIGURES.....	ix
LIST OF TABLES	xiii
1. INTRODUCTION.....	1
1.1 Research Motivation and Objectives	2
2. LITERATURE REVIEW	4
2.1 Minimum Quantity Lubrication.....	4
2.2 MQL generated by Mist Generator	5
2.3 MQL generation by coaxial tube	8
2.4 Types	9
2.5 Comparison between dual & single channel MQL systems.....	11
2.6 External MQL Characterization	12
2.7 Internal MQL characterization	13
2.8 Contact Angles	19
2.9 Critical parameters for performance of MQL systems.....	22
2.10 Machining in MQL	22
2.11 Health Concerns.....	27
3. EXPERIMENTS	29
3.1 Equipment & Software	29

3.2	Procedure	30
3.2.1	Plastic Tool Adapter	30
3.2.2	Calibration	33
3.2.3	Contact Angle	36
3.2.4	Collection of droplets	37
3.3	Droplet characterization using APS 3321	41
3.4	Micromilling	42
3.5	Metrology	46
3.6	Air flow velocity	48
4.	RESULTS AND DISCUSSION	50
4.1	Contact Angle	51
4.2	Air Flow Velocity	51
4.3	Droplet Characterization	58
4.4	Micromilling of Inconel 718	73
5.	CONCLUSIONS AND RECOMMENDATIONS	85
	REFERENCES	86
	APPENDIX A	89
	APPENDIX B	90
	APPENDIX C	95
	APPENDIX D	96

LIST OF FIGURES

Figure 1 Machining with (a) Flood Cooling (b) Minimum Quantity Lubrication	5
Figure 2 Simplified Impactor Model.....	6
Figure 3 Co-axial tubes carrying lubricant and compressed air separately.....	8
Figure 4 Types of MQL system	9
Figure 5 (a) External MQL, and (b) Internal (Through the tool) MQL	10
Figure 6 Internal MQL Systems (Top.) Internal Single Channel MQL (Bottom.)	
Internal Dual Channel MQL	11
Figure 7 Experimental Setup.....	12
Figure 8 Mist flow rates for different cross sectional configurations of tool holder	14
Figure 9 Mist flow rate against rpm for internal single channel MQL	16
Figure 10 Flowrate vs spindle speed at three flowrates	17
Figure 11 Traces of airborne particles from dual channle (internal).....	18
Figure 12 Interfacial tension force vectors.....	19
Figure 13 Contact angles of different lubricants on 316L stainless steel.....	21
Figure 14 (a) Variation in surface finish (b) Variation of tool diameter at feed rate of	
2.5 $\mu\text{m}/\text{flute}$	24
Figure 15 Tool wear plotted against cutting time	25
Figure 16 8 regions on ABS plastic measured before and after exposure to lubricant	31
Figure 17 Sectional view of nozzle adapter and original nozzle.....	33
Figure 18 (a) Droplet on glass slide (b) 8 bit image of the droplet (c) Analyzed image	
showing the droplet outline	35

Figure 19 Optical image of 0.2 μ L Coolube 2210 EP droplet on glass	37
Figure 20 (a) Unist Micromist Lubrication System (b) Experimental setup for droplet collection	39
Figure 21 (a) Experimental setup for machining (side view) (b) Tool path for milling (top view)	45
Figure 22 (a) Measurement of Surface Roughness (b) Measurement of Profile Roughness	47
Figure 23 Moving path of anemometer probe.....	49
Figure 24 (a) Exit air velocity (m/s) at 550 kPa for rough nozzle adapter and smooth nozzle adapter (b) Exit air velocity (m/s) at 275 kPa for rough nozzle adapter and smooth nozzle adapter	52
Figure 25 Air flow velocity along nozzle axis	55
Figure 26 MQL flow (air + lubricant) velocity along the nozzle axis	55
Figure 27 (a) Exit MQL (air + lubricant) droplets velocity (m/s) at 550 kPa for rough nozzle adapter and smooth nozzle adapter (b) Exit MQL droplets (air + lubricant) velocity (m/s) at 275 kPa for rough nozzle adapter and smooth nozzle adapter.....	56
Figure 28 Resulting microdroplet images with (I) from original nozzle, (II) rough nozzle, and (III) smooth nozzle.....	59
Figure 29 Micro droplet images for sample collected at 550 kPa using the original nozzle (a) as deposited on glass, (b) after bitmap conversion.....	60

Figure 30 Droplet distribution at 276 kPa with (a) with smooth nozzle (b) with rough nozzle (c) original nozzle	62
Figure 31 Droplet distribution at 415 kPa with (a) with smooth nozzle (b) with rough nozzle (c) original nozzle	63
Figure 32 Droplet distribution at 550 kPa with (a) with original nozzle (b) with rough nozzle (c) smooth nozzle.....	64
Figure 33 Effect of air pressure and nozzle surface on (a) airborne droplet diameters in MQL, and (b) their standard deviations.	66
Figure 34 Droplet distribution generated using APS (a) without nozzle adapter (b) with rough nozzle adapter.....	69
Figure 35 Moody Diagram	70
Figure 36 Inconel 718 (a) in powder form, and (b) on xy-plane surface after SLM.....	73
Figure 37 10 milled slots on Inconel 718.....	74
Figure 38 Area surface roughness when milling in MQL from a (a) rough nozzle, and (b) smooth nozzle.	76
Figure 39 Area surface roughness when milling with air pressure of (a) 275 kPa and (b) 550 kPa.	77
Figure 40 Profile roughness when milling with air pressure of (a) 275 kPa and (b) 550 kPa.	79
Figure 41 Profile roughness when milling in MQL from a (a) rough nozzle, and (b) smooth nozzle.....	80
Figure 42 Cumulative tool wear when milling in MQL from (a) rough nozzle, and (b)	

smooth nozzle.....	82
Figure 43 Insignificant burr at cumulative milling distance of 5 mm, but lots of burr (label *) are formed after 135 mm milling distance. Note the narrower slot width of the latter	84
Figure 44 Design of Nozzle Adapter.....	89
Figure 45 UNIST MQL Lubrication System	90
Figure 46 Olympus STM 6 Microscope.....	91
Figure 47 Alicona InfiniteFocus Microscope	93

LIST OF TABLES

Table 1 Comparison between dual and single channel MQL	11
Table 2 Compatibility of ABS plastic with lubricant.....	32
Table 3 Parameters from the extracted image	35
Table 4 Micromilling tool	42
Table 5 Experimental iterations	44
Table 6 Machining parameters	44
Table 7 R_a Calibration Results using Mitutoyo Surface Standard $R_a= 2.95 \mu\text{m}$	50
Table 8 Projected diameters and contact angles for 5 samples at 0.2 μL and 0.3 μL volumes of Coolube 2201 EP on glass.....	51
Table 9 Airborne microdroplets' mean diameters and standard deviations (in parenthesis).....	66
Table 10 Total tool wear (slot width change, μm)	83
Table 11 HASS OM2 CNC Milling Machine Technical Specifications	92
Table 12 Technical specifications of Alicona InfiniteFocus Microscope.....	93

1. INTRODUCTION

Traditional machining processes use sharp cutting tools and mechanical means to shape raw stocks into desired profile by removal of material. Heat is generated due to friction of chip against tool rake face and shearing of workpiece material. This leads to accelerated tool wear, built up edges (BUEs) and surface defects on the workpiece resulting in higher expenses due to shorter tool life, poor surface finish and surface defects that may lead to the failure of workpiece.

Flood cooling can be used to reduce the generated heat in machining. Large amount of coolant is applied to cool down the tool and workpiece while removing chips. Flood cooling uses large quantities of coolant along with additional equipment needed to recycle it. It may lead to thermal shock in tools and cause tool failure. Through tool lubrication is another way to cool the tool and the workpiece. The coolant is supplied through internal channels of the tool. This ensures that the coolant reaches the tool-workpiece interface and reduces the cutting temperature. Although coolant/lubricant is required in machining, applying a large amount of cutting fluid would raise the manufacturing cost while having a negative impact on the environment. Due to the downsides of conventional lubrication, use of minimum quantity lubrication (MQL) –or near dry lubrication– has been gaining momentum not only because of the above mention effects but also because of tool life improvement when properly applying MQL. Many researchers have shown the effectiveness of MQL on tool life enhancement in

machining tests such as turning and milling with externally applying MQL but limited study was published when MQL is applied through the tool.

The Inconel 718 (IN718) is a super alloy which is being widely used in aerospace, oil and gas, or nuclear industries for its suitability in high temperature environments. This alloy is difficult to machine due to its high strength, hot hardness and high chemical affinity to most materials used for tooling. 3D printing is gaining momentum from a rapid prototyping technique to a production tool that can be used to manufacture parts that were difficult to manufacture using conventional methods. These parts then can then be machined to get the final profiles. Effective lubrication is important to machine Inconel.

1.1 Research Motivation and Objectives

Use of additively manufactured Inconel parts is gaining momentum in aerospace, oil and gas and nuclear industries. Although significant information was published on machining extruded or rolled IN718, there is yet a study on machining of additively manufactured Inconel. Similarly, most published literatures were seen for externally applied MQL and limited work was found on characterization of through-tool MQL and its effect on machinability. This research study fills the gap by simulating through-tool MQL, characterizing the through-tool MQL droplets and applying the results on micromilling of selective laser melted (SLM'ed) IN718.

The objectives of this study were to:

1. Simulate through-tool MQL and experimentally characterize the lubricant droplets

2. Analyze the effect of surface roughness of the nozzle on the drop size and distribution, and exit air velocity.
3. Determine the effect of MQL droplets when micromilling of 3D printed IN718.

2. LITERATURE REVIEW

This section reviews:

- i. The principle involved in generation of MQL and different types of MQL systems. Droplet characterization and droplet distribution.
- ii. Contact angles of various lubricants and effect on machinability.
- iii. Effects of MQL on machining in both macro and micro scales.

2.1 Minimum Quantity Lubrication

Minimum quantity lubrication, synonymously known as near dry machining is becoming common as an alternative to flood cooling. Both methods are shown in Figure 1. This technique uses oil and a stream of compressed air to form mist. This atomized spray is then applied to the tool workpiece interface. MQL forms a layer of lubricant on the workpiece tool interface and lubricates the interface, reducing the amount of heat caused due to friction.

Volumetric flow rate in MQL varies between 5-100 mL/hr compared to 19 L/min required for flood coolant (Dasch and Kurgin, 2010). MQL does not need the recirculation system required for flood coolant. It deposits lubricant on the workpiece, is evaporated or taken away along with the chips.



Figure 1 Machining with (a) Flood Cooling (b) Minimum Quantity Lubrication (Reprinted from UNIST Coolubricator, n.d.)

The purpose of oil-based fluids used in MQL is to reduce friction as they do not have the high specific heat capacity of water-based coolants. They can be effective if the droplets cover the tool chip and tool workpiece interface. To ensure coverage of the desired regions for lubrication, droplet size and distribution needs to be determined in terms of the input parameters. Small droplets will effectively reach the workpiece tool interface but droplet smaller than a certain diameter would be carried away and evaporated in air due to its low mass and low settling velocity.

2.2 MQL generated by Mist Generator

Impactor plate was used to filter out droplets larger than a certain diameter from the flow stream. The cross section of an impactor can be seen in Figure 2. The droplets coming through the nozzle were assumed to have a constant velocity and were considered to be moving along the streamline. On exit, the streamlines followed an arc centered at A. As particles exited the nozzle, a centrifugal force moved them towards the impaction plate. All droplets shift a small distance “ Δ ” towards the plate where (Hinds, 1999)

$$\Delta = \frac{\pi}{2} \tau U \quad (1)$$

Where

τ : relaxation time (s)

U : free stream velocity (m/s)

Δ : distance moved by the particle towards the plate (m)

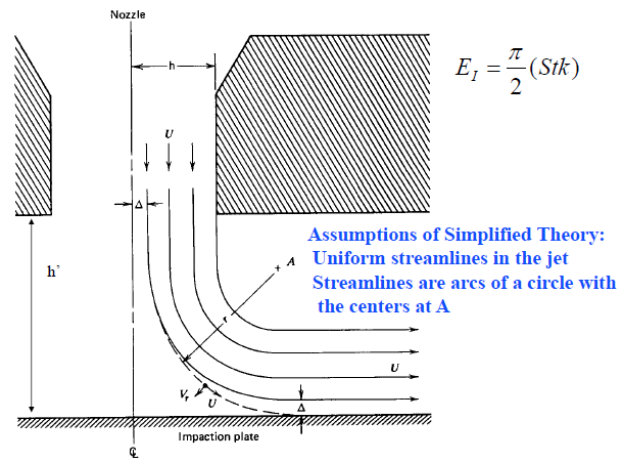


Figure 2 Simplified Impactor Model (Reprinted from Hinds, 1999)

Droplets lesser than the distance of Δ from the plate will get deposited on the impaction plate. If the distance between the impaction plate and nozzle is decreased and other parameters are kept constant, smaller particles will deposit on the impaction plate. Increasing the velocity of the particles will also result in larger Δ leading to the deposit of particles with smaller diameter on the impaction plate.

The following mist generation method uses the preceding idea to generate droplets and control their diameters.

The lubricant was stored in the tank and pressurized air was introduced via tube. The compressed air reached nozzle via orifice creating a negative pressure at the nozzle.

This negative pressure siphoned the lubricant into the nozzle and a multiphase mixture is sprayed from the nozzle into generator. The droplet size varies from 5 μm to 70 μm in diameter with the count median diameter of the distribution being 35 μm .

An adjustable valve, faced the generation nozzle. Adjusting this valve towards the right decreased its distance from the generation nozzle, reducing the median diameter of lubricant's droplets.

The droplets were sprayed through the generation nozzle onto the buffer valve. Sprayed particles below a certain diameter dispersed after their impact on the buffer valve due to their smaller mass. Droplet above this diameter impacted the buffer valve and were collected in the tank below. The mean diameter of droplets was reduced by decreasing the distance between the generation nozzle and the buffer valve resulting in decrease of median diameter of the droplets. Majority of droplets were reduced to having diameter of less than 35 μm with a median diameter of 10 [Sakaida et al., 2006].

The mist of droplets was then introduced in the particle classifier. Increase in velocity of the droplets will result in a decrease of the diameter of the size of droplets of mist as increased velocity results in increase of distance Δ . The flow rate of the mist introduced into the particle classifier was adjusted by varying the adjustment screw. Particles with the larger diameter deposited on the impaction plate due to their high momentum and were collected in form of liquid. The liquid was returned to the tank through the return pipe. Droplets with smaller diameter were discharged as micromist through outlet port and sprayed on the workpiece being machined. The size of these

droplets was lesser than 10 μm in diameter. Maximum diameter of droplets at output was reduced to a median of 7 μm with the maximum diameter being around 10 μm .

2.3 MQL generation by coaxial tube

The second method for the generation of MQL micromist consists of a delivery method through coaxial tubes. The inner tube carries the lubricant oil with outer tube carrying the compressed air. Coaxial tubes transport compressed air and lubricant separately and both fluids are allowed to mix right before the output nozzle (Figure 3). Compressed air breaks down the lubricant to form droplets which are then deposited onto the workpiece.

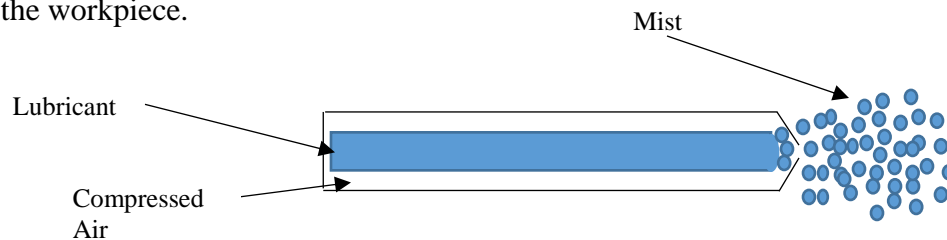


Figure 3 Co-axial tubes carrying lubricant and compressed air separately

Mist generation right before the nozzle ensures a consistent size of the droplets irrespective of the length of the tube. Mist travelling through a long tube will have droplets accumulated along the bends of the tube and may drip as “blobs” of lubricant effecting the smooth spray pattern of the aerosol. The second method of aerosol generation also ensures that any adjustments to the flow rate and air pressure are immediately propagated to the output at the nozzle.

2.4 Types

MQL can be categorized into internal MQL and external MQL. Internal MQL can be further subdivided into internal single and dual channel MQL systems as shown in Fig.4.

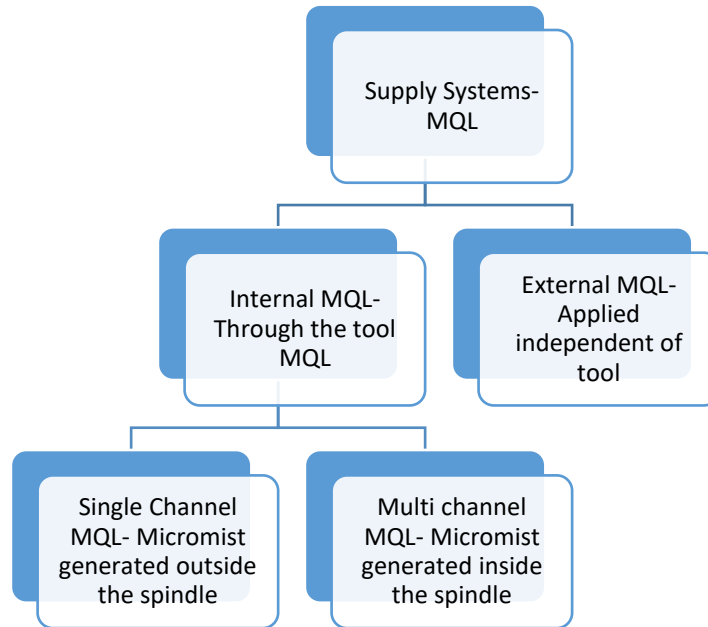


Figure 4 Types of MQL system

An External MQL system (Figure 5a) sprays the droplets on the workpiece from the nozzle located near the tool workpiece interface. This is the simplest and cheapest form of MQL systems as it requires no special tooling to work and can be applied to existing machining systems without any modifications. For operations such as tapping and drilling, external MQL systems were only favorable if the ratio of depth of hole to the diameter of hole was lesser than 3 (Chetan et al., 2015). If only one nozzle is used during the external application, shadowing effect may occur. This will result in no

lubricant reaching the opposite end of the tool and multiple nozzles will be needed to ensure lubrication of the entire tool-workpiece interface. Another important factor affecting the efficient working of external MQL system is the distance of nozzle from the tool workpiece interface. Li et al. (2015) observed a decrease in air speed from 35 m/s measured at the nozzle to 30 m/s at 10 cm away from nozzle at pressure of 200 kPa.

Assuming a large tool is used, an internal MQL system (Figure 5b) directly supplies the aerosolized lubricant through the tool into the workpiece. This ensures that the tool workpiece interface is constantly supplied with lubricant. These systems can be used to ream, drill and tap holes having high aspect ratio. These systems require high costs of implementation on the existing machines as specialized spindles and drill bits are required to carry the lubricant inside them.

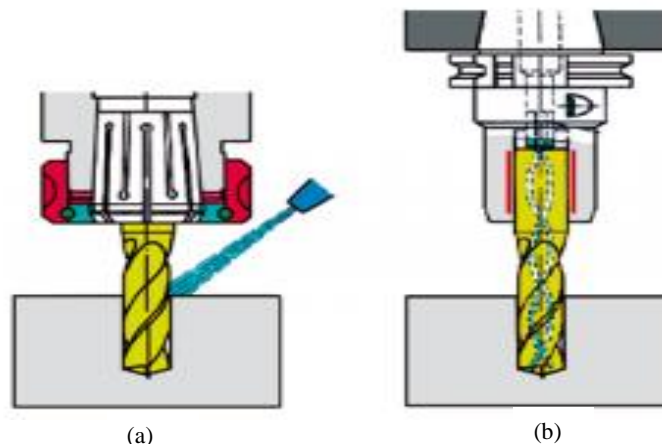


Figure 5 (a) External MQL, and (b) Internal (Through the tool) MQL (Reprinted from Weinert et al., 2004)

Internal MQL systems can be subdivided into dual and single channel MQL systems (Figure 6). Internal single channel MQL systems produce the mist outside the

spindle which then travels through the spindle and the tool. Dual channel MQL systems use separate channels to carry compressed air and lubricant to the tool holder. After mixing at tool holder to form the micromist, they travel through the tool and exit at the workpiece-tool interface. Internal MQL systems use rotary unions to allow the flow of compressed air and lubricant by providing a seal between the rotating spindle and the supply passage. Table 1 compares single and dual channel MQL systems.

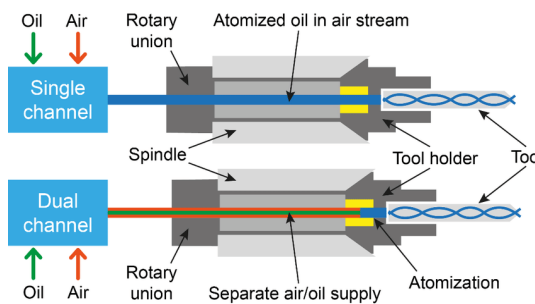


Figure 6 Internal MQL Systems (Top.) Internal Single Channel MQL (Bottom.) Internal Dual Channel MQL (Reprinted from Tai et al., 2014)

2.5 Comparison between dual & single channel MQL systems

Table 1 Comparison between dual and single channel MQL Systems [Adapted from Dwuletcki, 2015]

Criteria	Single Channel System	Dual Channel System
Lubricant Feed	Dependent on rotational speed of spindle as the mist has to travel through spindle and tool	Not heavily dependent on the rotational speed of the tool as the mist is formed just before entering the tool
Rotational Speed	16,000 rpm maximum	40,000 rpm maximum
Bore/Air Size	Affects maximum feed	Does not affect maximum feed
Reaction Time	Slow	Fast
Air Pressure	>500 kPa	> 400 kPa
Fluid Transport	Via transfer lines to the target area	Via CNC Centers & machine tools

2.6 External MQL Characterization

Park et al. (2010) used the setup shown in Figure 7 to characterize the droplets produced through external MQL using confocal laser scanning microscopy.

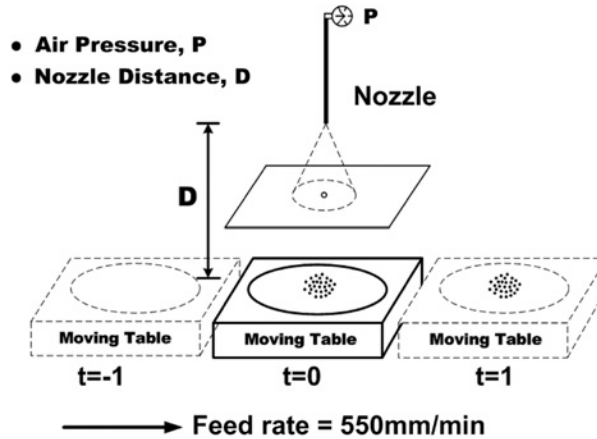


Figure 7 Experimental Setup (Reprinted from Park et al., 2010)

The aerosolized lubricant was deposited on the silicon wafer so that the diameter and shape of the droplets could be extracted using the microscope. Flowrate for the lubricant was adjusted to 3.2 mL/min and a screening plate with a hole was used to ensure that droplets did not overlap after exiting the nozzle. The size of the screening hole was set to 0.8 mm after multiple experiments as the diameter of droplets did not decrease below this diameter of the hole. Distance ‘D’ of the nozzle from the wafer and the air pressure ‘P’ were changed while maintaining a constant flowrate of 3.2 mL/min and the variation in size and distribution of the droplets was analyzed.

- The size of the droplets decreased with increasing pressure. Droplets covered the maximum surface area fraction of 15.1 % when the highest pressure was applied while the distance between the plate and the nozzle was kept minimum.

- Reduction in surface area covered by the droplets at higher pressure was steeper than the reduction at lower pressures. The decrease of the droplet size from 12.93 μm to 11.32 μm with increase in pressure from 27.5 kPa to 82.7 kPa was contributed to the fact that the stopping distance of the particles was reduced leading to lesser particles getting deposited on the wafer. A small distance between the nozzle and the moving table at higher pressure ensured maximum amount of droplets getting deposited on the workpiece for better lubrication.

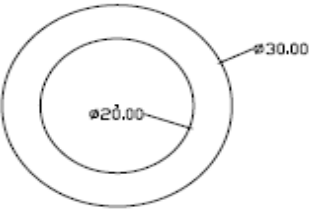
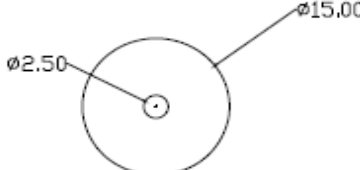
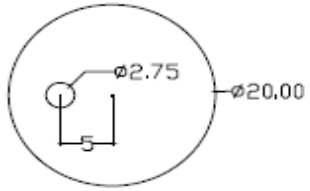
Sai et al. (2015) characterized the droplet characteristics from an external nozzle using experimental and computational method. The authors used water and air to form the micromist for simplification of computational model. They observed that at the flowrate of 50 mL/h, the mean diameter of the droplets reduced from 10 μm to 7 μm when the pressure was increased from the 0.3 MPa to 0.5 MPa. Increase in pressure to 0.6 MPa reduced the mean diameter of the droplets to 6 μm . The increase of flowrate to 500 mL/h didn't have any significant effect on the particle size.

2.7 Internal MQL characterization

Dasch and Kurgin (2010) characterized internal MQL using a machining enclosure. Measurements were done in a duct made out of stainless steel leading from the enclosure to the mist controller unit. Concentration of aerosolized lubricant were measured continuously by DataRAM continuous particle monitor. A 13 stage MOUDI cascade impactor was used to generate the droplet size distribution of MQL. The impactor could measure particles having diameters between 0.03 μm to 18 μm . Filter for

each stage was weighed after the experiment to determine the mass median droplet diameter.

Internal, single channel MQL with mist being generated outside the machine was characterized first. Tool holders with three different cross sectional variations were tested. When the internal diameter of the tool holder was reduced from 20 mm to 2.5 mm, the flowrate of the mist through the tool holder increased from 1.9 mL/h to 18 mL/h. When the internal hole was given an offset of 5 mm from the center (Figure 8), the flowrate increased to 24 mL/h. The experiments concluded that tool holder's geometry had an effect on the effective transfer of mist to the tool. Fragility of aerosolized droplets meant that they were more sensitive to the tool holder's cross sectional area than flood coolant and could get lost on the surface of the geometry.

Toolholder	Toolholder cross section (units are mm)	Mist flow at 0 rpm (mL/h)
1		1.9
2		18
3		24

Note: The internal circles represent openings in each toolholder through which the mist flowed.

Figure 8 Mist flow rates for different cross sectional configurations of tool holder (Reprinted from Dasch and Kurgin, 2010)

Tool holder 3 was used in the experiments as it gave the best output flow rate of 24 mL/h out of the three configurations tested. The aerosolized lubricant has to pass through spindles rotating at high speeds. High spindle speeds lead to higher centrifugal forces being experienced by the droplets. Droplets experience varying forces depending on their position from the center of rotation giving rise to relative velocity among the droplets. This causes kinematic coagulation of droplets. These coagulated droplets are thrown to the sides of the tool holder or eject as big blobs of liquid contributing to highly varying measurements. The following figure shows the change in measured mist flow rate at the output plotted with increasing rotational speed of the spindle. It can be seen that the flow rate falls rapidly as the rotational speed is increased. For a rotational speed of as low as 2500 rpm, the flow rate has decreased to only 3 mL/hr showing adverse effects of rotational speed on flow rate (Figure 9).

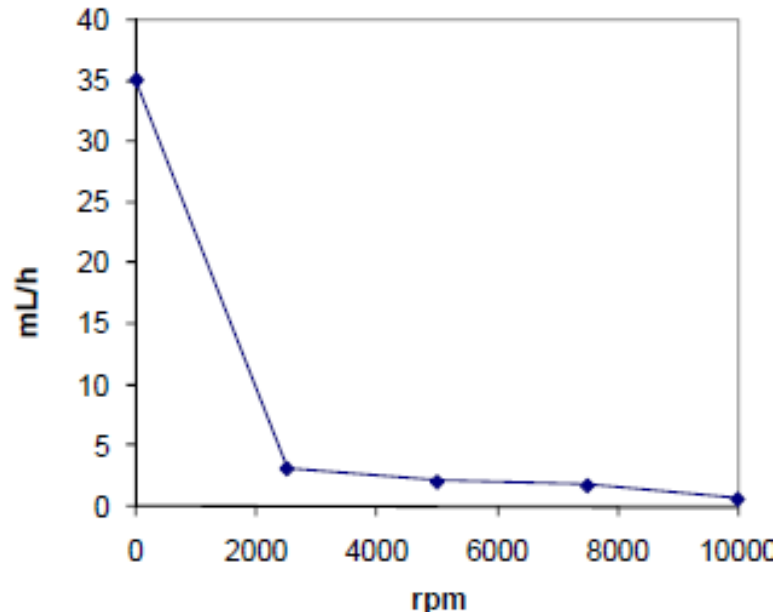


Figure 9 Mist flow rate against rpm for internal single channel MQL (Reprinted from Dasch and Kurgin, 2010)

Internal dual channel MQL uses separate channels to transfer compressed air and lubricant from the source to the tool holder. Dasch and Kurgin (2010) tested three different flowrates to determine the effect of rotational velocity of the spindle on the mist flowrate measured at the exit. A decreasing trend in the measured flowrate was observed with the increase in rotational velocities. The rate of decrease was lesser than that for internal single channel MQL as the mist was generated just before the tool and had to travel shorter distance. This dampened the effect of rotational velocity on coagulation of mist droplets.

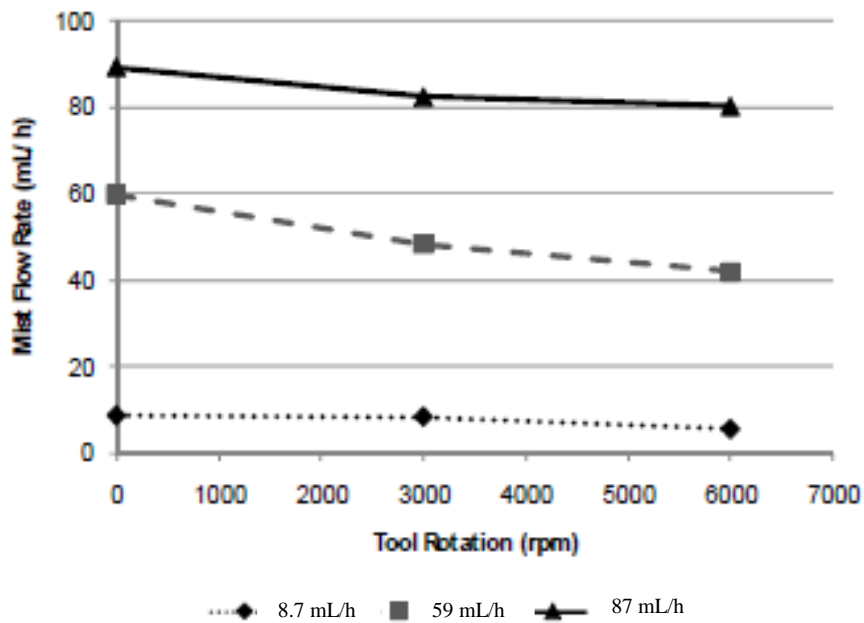


Figure 10 Flowrate vs spindle speed at three flowrates (Reprinted from Dasch and Kurgin, 2010)

The setup also included a continuous particles counter to measure the concentration of mist droplets in air. The measurements were done with the tool rotating in air, during its rotation in pre drilled holes and while machining. Concentration of particles in air for these conditions is plotted in Figure 11.

Revolutions of tool in air generated the highest concentration at 1.7 mg/m^3 . During rotation of tool inside the pre drilled holes, the measured concentration dropped to 0.57 mg/m^3 due to collection of the droplets inside the holes. The measured concentration rose to 0.74 mg/m^3 while drilling due to dispersion of file aluminum particles in the air stream (Dasch and Kurgin, 2010).

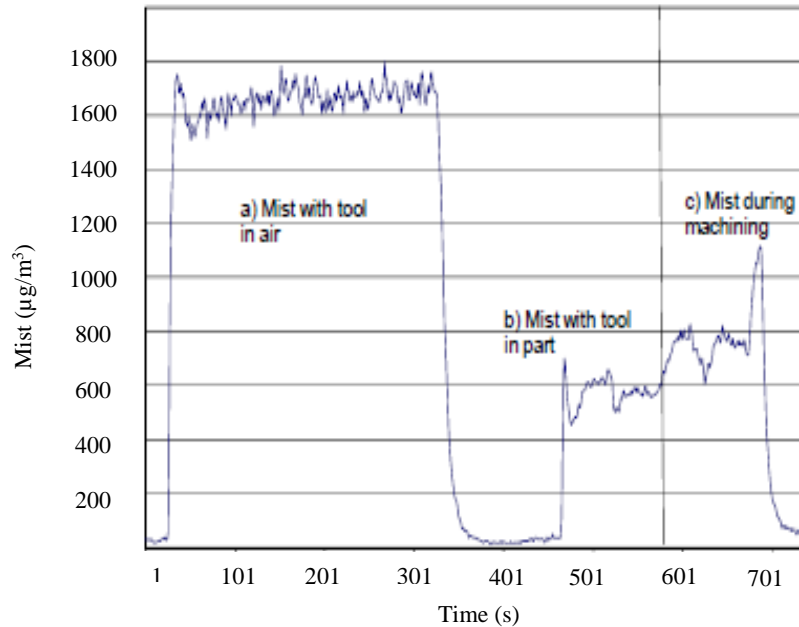


Figure 11 Traces of airborne particles from dual channel (internal) MQL (Reprinted from Dasch and Kurgin, 2010)

The distribution of droplets for wet application (external MQL) peaked around the 6-10 μm region with negligible mass lying in the submicron region. For the internal, single channel application, droplets of MQL were much smaller in size with the mass distribution peaking between 1-2 μm . Quarter of the distribution lied in the submicron region showing the smaller size of droplets for internal, single channel MQL when compared to internal, dual channel MQL. The dual channel MQL recorded the most mass for droplets in 3-5 μm range, with only 11% of the droplets falling in submicron range. Mass median diameter is defined as the droplet size which divides the mass distribution into two equal halves. It was smallest for the single channel MQL. The largest diameter were generated by wet application, followed dual channel MQL. Mass median droplet diameter was in order (Dasch and Kurgin, 2010):

$$\text{Internal, Single} < \text{Internal, Dual} < \text{Wet}$$

2.8 Contact Angles

Wettability describes the characteristic of the fluid to spread out to cover the workpiece and the machining tool. Contact angle (θ) is a common parameter used to measure the wettability of a surface of the deposited lubricant. It is the angle between the droplet and the surface in thermal equilibrium with one another and the ambient gas phase. A lower contact angle indicates the higher wettability of the fluid.

Young's equation relating the interfacial surface tensions of the three phases of matter to the contact angle θ is (Tai et al. 2011):

$$\gamma_{SG} = \gamma_{SL} + \gamma_{LG} \cdot \cos \theta \quad (2)$$

Where:

γ_{SG} : interfacial tension force vector between solid and gas (N/m)

γ_{SL} : interfacial tension force vector between solid and liquid (N/m)

γ_{LG} : interfacial tension force vector between gas and liquid (N/m)

θ : Contact angle ($^\circ$)

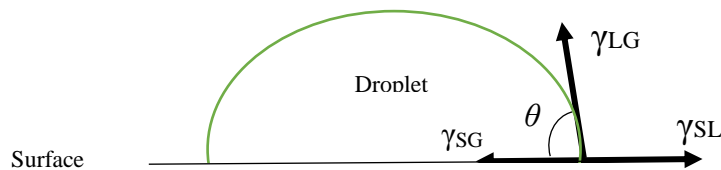


Figure 12 Interfacial tension force vectors

Liquids with lower contact angles ensure that droplet of the lubricant can spread out covering more surface area on the workpiece contributing to better machining, longer tool life and smoother finish of the workpiece.

Sessile drop of known volume was deposited on the glass slide and used to determine the contact angle using equation (3) (Li et al., 2015).

$$V' = \frac{\pi P^3 (2 - 3\cos\theta + \cos^3\theta)}{24(1 - K\cos^2\theta)^{1.5}} \quad (3)$$

$$d = \left(\frac{6V'}{\pi}\right)^{1/3} \quad (4)$$

Where,

P : projected drop diameter (mm)

V' : droplet volume (mm³)

θ : contact angle (°)

d : diameter of the airborne droplet (mm)

K : 1 for $\theta < 90^\circ$; $K=0$ for $\theta > 90^\circ$

It was assumed that:

- The volume of the droplet was very small
- The effects of gravity on the droplet were neglected
- Droplets were formed on a flat and polished surface

Li et al. (2015) used water along with different lubricants to determine their contact angles and wettability on 316 L stainless steel. Figure 13 shows the results of the conducted experiments. Droplets having same volume of Coolube 2210 EP covered different areas on the steel plate indicating their varying contact angles and wettability.

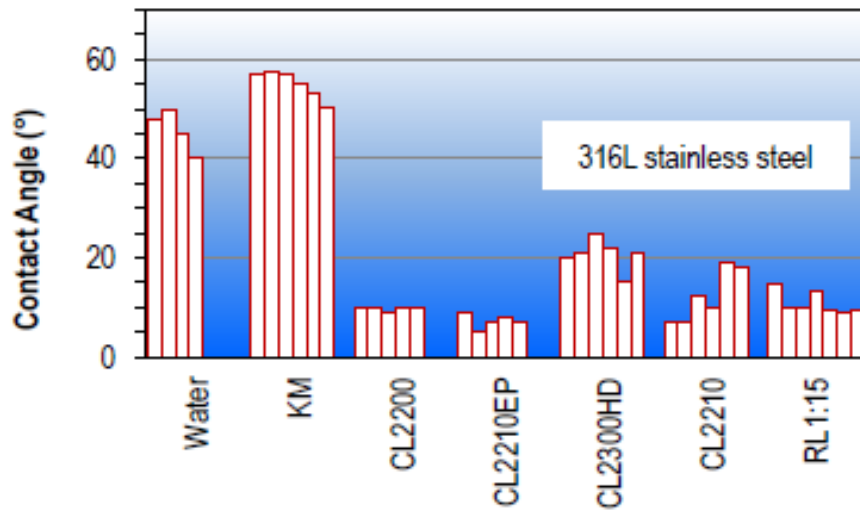


Figure 13 Contact angles of different lubricants on 316L stainless steel [Reprinted from Li et al., 2015]

The lubricants Coolube 2210 EP and Coolube 2200 having lower contact angles of 10° and 5° respectively, are indicating larger covered surface areas in Figure 13.

Li et al. (2015) reported contact angles of Coolube 2210EP was about $5-10^{\circ}$ on 316L stainless steel, pure titanium, and polished tungsten carbide. Tai et al. (2011) compared tribological and physical properties of commonly used MQL fluids and their performance during drilling and reaming operations with through-tool MQL. Their testing proved that straight oil based lubricant used for MQL was better in terms of lubrication and wettability but lacked the heat removal properties inherent to water based fluid. Contact angles of vegetable based MQL lubricants on tungsten carbide tool material were in the range $7.6-26.5^{\circ}$, whereas for water based lubricant it increased to approximately 36° .

2.9 Critical parameters for performance of MQL systems

Following parameters can ensure effective lubrication of tool and workpiece for improved machining.

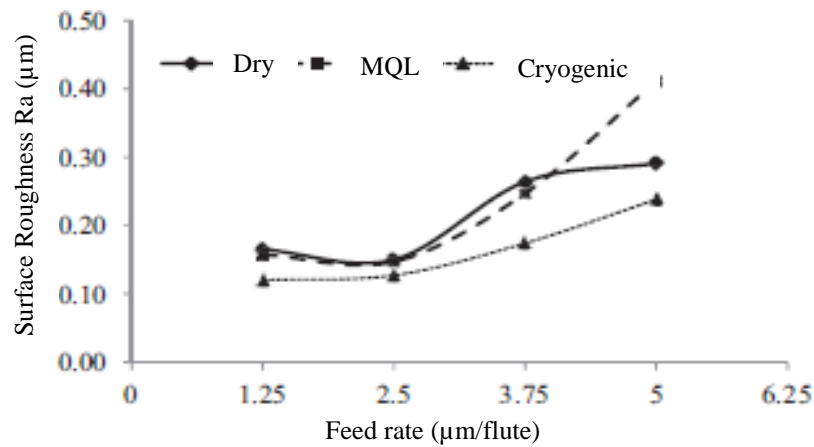
- The contact angle between the droplet of the lubricant and the surface of the workpiece or tool should be large to ensure maximum coverage by the lubricant and effective lubrication.
- An even and thin layer should be ensured on the surface of workpiece, tool and tool workpiece interface. Lubricant with low surface tension between liquid and solid promotes capillary movement to bring lubricant to tool/chip interface.
- Application of high pressures results in excessive misting of lubricant. Small particles have small settling velocities making it difficult for them to get deposited on the workpiece and lubricate it. These particles evaporate quickly without lubricating the surface.
- The use of flood coolant ensures that the chips created from machining are carried away with the coolant which is not the case in application of MQL. Workpiece should be oriented in a position guaranteeing easy removal of chips. Intermittent blasts of compressed air can be programmed to make sure that the chips are regularly cleaned up and do not clog the tool.

2.10 Machining in MQL

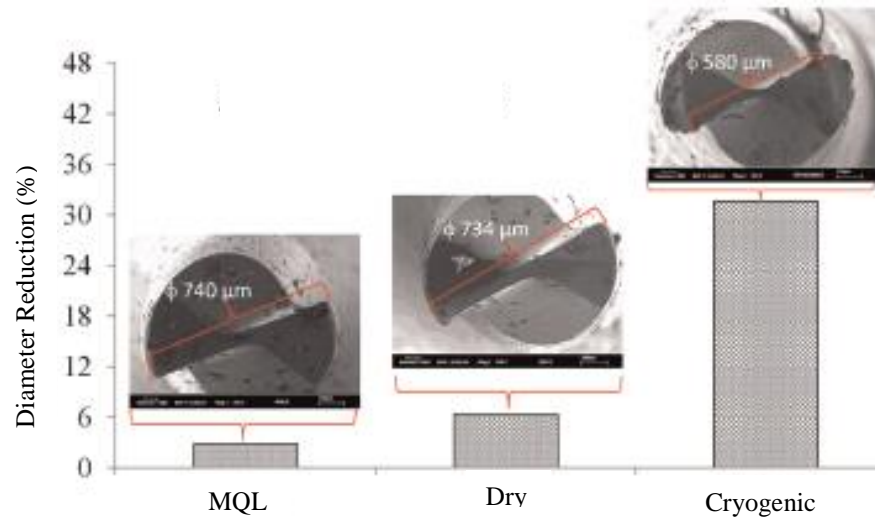
The super alloy IN718 has been widely used in aerospace, oil and gas, or nuclear industries for its suitability in high temperature environments.

Ucun et al. (2014) determined the effects of MQL and cryogenic pre cooling on the micromachining performance of IN718. Coolube 2210 was used as the lubricant oil and MQL was applied at a flowrate of 150 mL/h. AlCrN- coated tool was used for micromilling. Machining was done at a constant spindle speed of 20,000 rev/min and a cutting speed of 48 m/min with the depth of cut being 0.1 μm , 0.15 μm and 0.2 μm . At the feed rate of 1.25 $\mu\text{m}/\text{flute}$, the surface finish obtained using cryogenic cooling was 0.12 μm compared to 0.16 μm obtained using MQL. Figure 14a shows that the difference in surface finish obtained using MQL and cryogenic cooling became more significant with the increase in feed rate. At the feed rate of 5 $\mu\text{m}/\text{flute}$ the surface finish using cryogenic cooling was 0.2 μm compared to approximately 0.26 μm using MQL.

At the feed rate of 2.5 $\mu\text{m}/\text{flute}$ the reduction in tool diameter was 3% for MQL compared to 31 % with the use of cryogenic cooling. The increased reduction in diameter along with the built up edges on the tool used under cryogenic cooling can be seen in Figure 14b.



(a)



(b)

Figure 14 (a) Variation in surface finish (b) Variation of tool diameter at feed rate of 2.5 µm/flute (Reprinted from Uzun et al.2014)

Uzun et al. (2013) investigated the effects of AlTiN, TiAlN/AlCrN and AlCrN tool coatings on the tool wear during micromilling of Inconel using MQL. Coolube 2210 lubricant oil was used for MQL. The operating frequency of the MQL system was kept at 200 pulse/min with a constant flowrate of 150 mL/h. The authors used $\phi 768 \mu\text{m}$ tool having two flutes at cutting speed of 48 m/min. They observed that at the feed rate of 5

$\mu\text{m}/\text{flute}$, there was only 3.75% in the reduction of tool diameter when MQL was used as compared to a reduction of 5.64% during dry machining.

Zhang et al. (2012) compared tool life and cutting forces for milling Inconel under dry machining conditions and with the application of MQL. MQL was generated at a pressure of 0.15 MPa with a lubricant flowrate of 8 ml/h. Down milling was done at 56 m/min speed, 875 rev/min rotational speed, and 0.5 mm axial depth of cut. Figure 15 shows the tool wear plotted against the cutting time. The wear under dry conditions was more than that measured with the use of MQL throughout the machining. After nearly 40 minutes of machining, the tool used under dry conditions wears rapidly, failing at approximately 43 minutes while the tool lubricated by MQL machines for 70 minutes without any anomaly. As the time machining time passed, the edges of tool used in dry machining became dull leading to a higher friction coefficient. This resulted in higher wear and ultimate failure of the tool edge. The authors reported that MQL enhanced tool life 1.57 times longer than when dry machining was done.

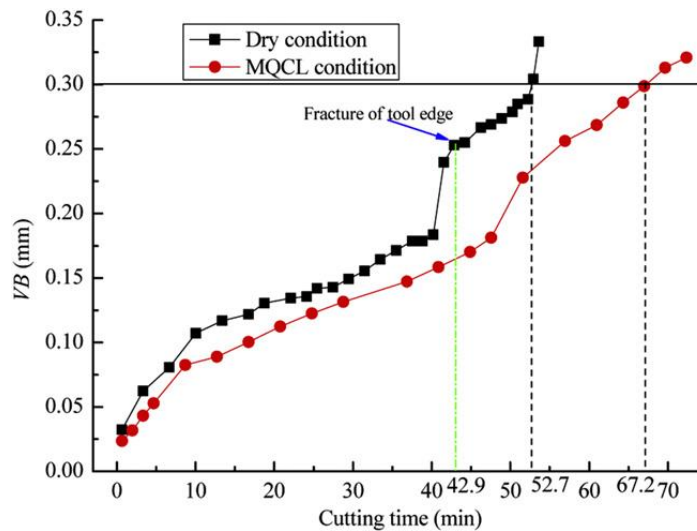


Figure 15 Tool wear plotted against cutting time (Reprinted from Zhang et al., 2012)

Thamizhmanii and Hasan (2009) observed the effect of MQL flowrate on surface roughness of machined IN718 and corresponding tool wear. Milling was done at 10, 20, 30 m/min cutting speeds at constant 0.15 mm/tooth feed rate. They reported an improvement in surface roughness from 0.6 μm to 0.4 μm when the flow rate of MQL was increased from 25 mL/h to 37.5 mL/h. Kayanak (2014) compared machining of Inconel using cryogenic cooling, MQL and dry machining. UNIST Coolube 2210 EP was used as the lubricant at an air pressure of 0.4 MPa. The flowrate was kept constant at 60 mL/h. The study concluded that the maximum temperature was above 800°C during dry machining, and reduced to nearly 600°C when MQL was used.

Although significant information was published for machining extruded or rolled IN718, there is yet a study on machining of additively built Inconel.

Kamata and Obikawa (2007) investigated tool wear and surface finish when turning Inconel. Tool coated with TiCN/Al₂O₃/TiN, TiN/AlN, and TiAlN were used in either MQL or flood coolant. Cutting speed range was 1-1.5 m/s, depth of cut was 0.1 mm, and feed rate was 0.1 mm/rev. The study showed that increasing MQL pressure from 0.4 MPa to 0.6 MPa decreased the tool life of TiN/AlN coated tools from 24 to 17 minutes. Such decrease of tool life was attributed to an increase in oxidation of the tool coating. However, the trend was reversed when grooving carbon steel in MQL: tool life improvement was observed with increasing MQL air pressure. There was no difference observed in the surface finish of Inconel. Obikawa et al. (2008) reported an increase in tool life from 24 minutes to 37 minutes for turning Inconel using MQL when

concentrated spraying of mist was done at a flowrate of 0.2 mL/h using a cover type nozzle.

Similarly, most published literatures were seen for externally applied MQL and limited research was published on through-tool MQL. This research study fills the gap by simulating through-tool MQL and applies the results on micromilling of selective laser melted (SLM'ed) IN718.

2.11 Health Concerns

PM_{2.5} are particles having diameter less than 2.5 µm and PM₁₀ are particles having diameter 10 µm or smaller. These particles are inhalable and due to their small size can get deposited in lungs overtime causing health problems. Occupational and health safety administration limits the mineral oil concentration of these particles on the machine floor to 5 mg/m³ for an eight hour time weighted average (OHSA, 1999). Anything greater than this would require the workers to use respiratory masks for protection. As MQL is a relatively new technology, the guidelines laid down for the mineral oil concentration are used. Anderson et al. (2004) reported lower mist concentrations around the machines using MQL than those operating with flood coolant. Moreover, Figure 11 shows us that the maximum concentration of mist in air is around 1.7 µg/m³ which is within the admissible limits. The costs of disposing the used coolant are also high due to legislations dictating their safe disposal (Stoll et al., 2008). Bennett (1992) reported skin disorders like dermatitis to workers who had prolonged exposure to cutting fluids. Hong

(2001) reported that 30 % of machining operators of an automobile plant developed dermatitis resulting from exposure to cutting fluid.

A study measuring the concentration of these particles during machining should be done to ensure that concentration is within the regulatory safety threshold set by Occupational and Health Safety Administration.

3. EXPERIMENTS

Experiments were conducted to:

- i. Simulate through-tool MQL and experimentally characterize the resulting liquid droplets due to different nozzle surface roughness and pressure.
- ii. Determine the outlet velocity of air and droplets due to different nozzle surface roughness and pressure.
- iii. Determine the effect of droplets on micromilling of 3D printed IN718.

Experiments were performed in two stages. The first stage characterized the resulting droplets due to different air pressures and surface roughness of a MQL nozzle. In the second stage, MQL at different operating conditions were applied when micromilling SLM'ed IN718. Tool wear and surface finish were used to assess the effectiveness of MQL.

3.1 Equipment & Software

Following is the list of equipment and software used to conduct the experimentation and measurements. Details are documented in Appendix B.

1. Aerodynamic Particle Sizer (APS 3321 TSI)
2. Alicona InfiniteFocus Micorscope
3. Arrow B754FM Air Regulator

4. Autoclavable Pipettor Micropipette
5. Coolube 2210 EP
6. HAAS OM 2 CNC Milling Machine
7. ImageJ Software
8. Kanomax Climomaster 6501 Anemometer
9. Olympus STM 6 Optical Microscope
10. Surface Standard (Mitutoyo, code no. 178-602)
11. Renishaw AM 200 Selective Laser Melting System
12. UNIST MQL Dispensing Unit

3.2 Procedure

3.2.1 Plastic Tool Adapter

Since an internal MQL system is complex, simulated through-tool MQL was performed based on an existing drill for internal coolant (Sanvik Coromat: Corodrill R840-0510-70-A1A 1220). It was assumed that:

- Micromist, formed by atomizing of lubricating oil and compressed air at a coaxial junction, flows through a hollow spiral channel to an edge of a cutting tool.
- The channel diameter is 3 mm, and 25.4 mm long.
- The exit droplet velocity along the channel axis dominates other component, i.e., its radial velocity component due to drill rotation is negligible.
- The micromist, flowing through a narrow channel nozzle, affects by the turbulent flow in the nozzle. This means the surface roughness of the nozzle inner surface channel would have an effect on the microdroplet sizes.

To ensure that the adapter perfectly aligned with the nozzle to eliminate leakage, the outer profile of the nozzle was measured using a coordinate measuring machine and the adapter was modelled accordingly using Pro Engineer.

An experiment was conducted to determine the suitability of ABS plastic to print the plastic nozzle adapter. The objective was to make sure that the plastic does not react with the Coolube 2210 EP when exposed to it for long periods of time. Following test was carried out to determine the compatibility of ABS plastic with Coolube 2210 EP.

1. A droplet of the Coolube 2210 EP was placed on a printed sample of ABS plastic.
2. The sample was left exposed to ambient environment for 24 hours.
3. Alicona InfiniteFocus microscope was used to measure the surface roughness of the surfaces of the regions before and after they were exposed to Coolube 2210 EP. Surface roughness was measured to ensure that the surface exposed to Coolube 2210 EP didn't react with it. Measurements were taken for various regions to increase the sample size.

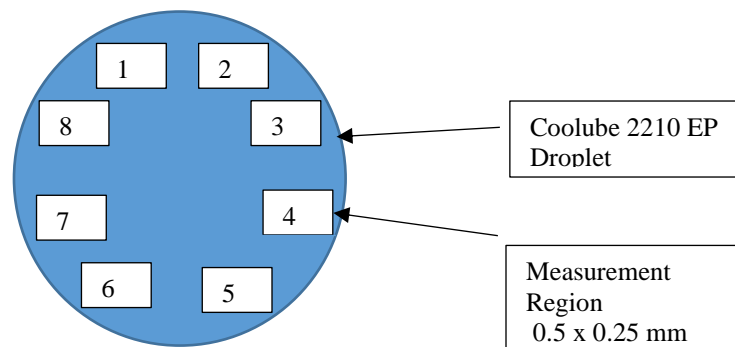


Figure 16 8 regions on ABS plastic measured before and after exposure to lubricant

Eight samples were taken on the circumference of the droplet exposed to the lubricant. Table 2 shows the surface finish of these regions before and after being exposed to the lubricant for 24 hours. No significant difference was observed on the samples after being exposed to the lubricant for 24 hours so it was concluded that ABS plastic was a good choice for the material of the adapter.

Table 2 Compatibility of ABS plastic with lubricant

	S_a of Unexposed Region (μm)	S_a of region exposed to lubricant (μm)
Region 1	4.165	3.665
Region 2	4.321	4.123
Region 3	4.249	3.883
Region 4	4.355	3.772
Region 5	4.142	4.270
Region 6	4.409	4.039
Region 7	4.271	4.270
Region 8	4.463	3.527
Average	4.294	3.950

The CAD model for the adapter is shown in the following figure. The detailed drawings for the adapter are in APPENDIX A.

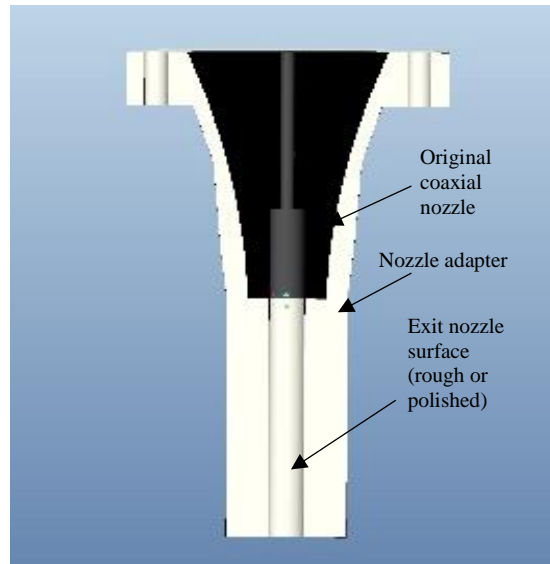


Figure 17 Sectional view of nozzle adapter and original nozzle

3.2.2 Calibration

The Olympus microscope was calibrated using the standard calibration slide. Accuracy of ImageJ software was verified to ensure that correct results were generated for the number and projected diameter of particles extracted from the glass slides and analyzed in the software. The accuracy of the software was verified in the following way.

1. A droplet of the lubricant was deposited on the glass slide.
2. The projected diameter of the droplet was measured using the caliper option in the software. The average caliper measurement was 1553 μm for the projected diameter of the droplet (Figure 18a).
3. The image was imported into ImageJ for analysis. The image was converted into an 8 bit image (Figure 18b)

4. The image was analyzed and the number of shaded regions, their location and the shaded area was extracted. (Figure 18c)
5. It was verified that the software was correctly able to identify the droplet boundary.
6. The area of the shaded region in mm² was used to determine the projected diameter of the droplet (Table 3). The shape was assumed to be a perfect circle and the formula for the area of circle was used to extract the projected diameter.

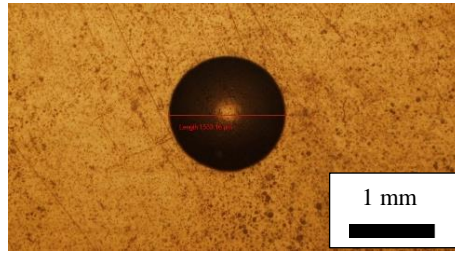
$$A = \pi P^2 / 4 \quad (5)$$

Where:

A: Projected area of the droplet (mm²)

P: Projected diameter of the droplet (mm)

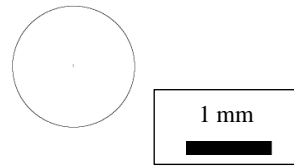
7. The projected diameter from the area was calculated to be 1523.4 μm having an error of 1.93% from the measured caliper reading through the caliper feature of microscope software. Multiple readings taken using the caliper feature in the software reduced the variations in the measurement. Thus, it was verified that the software was reading the images and giving the measurements correctly.



(a)



(b)



(c)

Figure 18(a) Droplet on glass slide (b) 8 bit image of the droplet (c) Analyzed image showing the droplet outline

Table 3 Parameters from the extracted image

Results										
File	Edit	Font	Results							
	Label	Area	Mean	Min	Max	Circ.	AR	Round	Solidity	
1	Image_1123-1.tif	1.823	255	255	255	0.902	1.010	0.990	0.994	

3.2.3 Contact Angle

The purpose of the experiments was to obtain the airborne diameter of the lubricant droplets. As the droplets are deposited on the glass slide, they spread preserving their volume but changing their morphology. The samples were to be collected on a glass slide so the contact angle between Coolube 2210 EP and glass was determined. A smooth surface glass slide was chosen for collection of droplets as it helped in getting better images of the collected droplets using Olympus microscope. Good image quality ensured accurate image analysis using ImageJ. Sessile drop of Coolube 2210EP was deposited on the glass slide. It was used to determine the contact angle. Contact angles were determined following the procedure below.

1. The glass slide was cleaned using ethanol and dried using compressed air.
2. A droplet of known volume of Coolube 2210 EP was deposited on the glass slide using an Autoclavable Pipettor micropipette. A set volume was sucked into the pipette from the lubricant container. The tip was rubbed around the container to get rid of the excess oil on the tip to ensure accurate deposition of droplet volume on the glass slide.
3. Five droplets of 0.2 μL were deposited on the glass slide. Another 5 samples were repeated with 0.3 μL using the micropipette. The high resolution pictures of the droplets on the glass slide were taken using Olympus optical microscope.
4. Caliper function of the software's microscope was used to measure the projected diameter of the droplets. Each measurement was repeated three times.

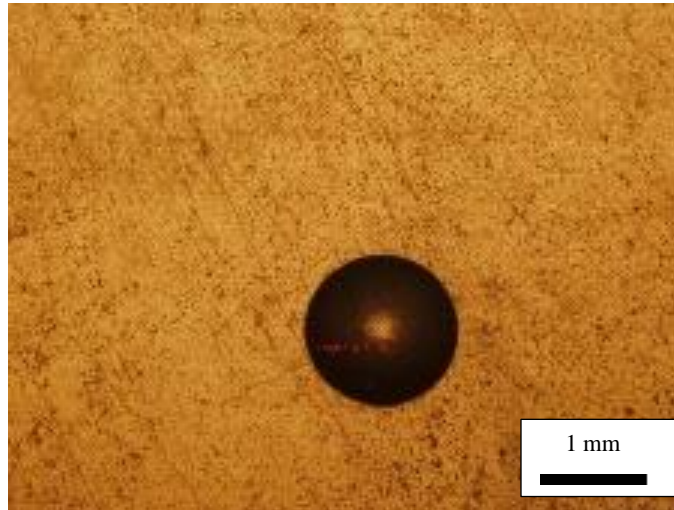


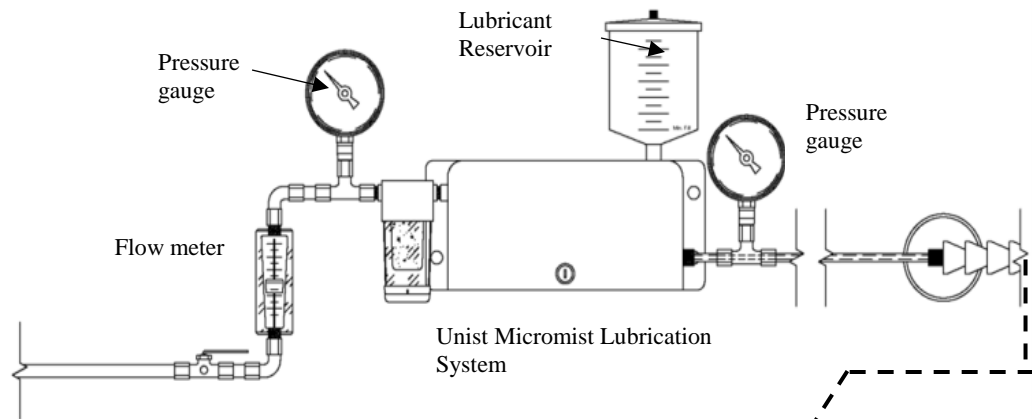
Figure 19 Optical image of 0.2 μ L Coolube 2210 EP droplet on glass

3.2.4 Collection of droplets

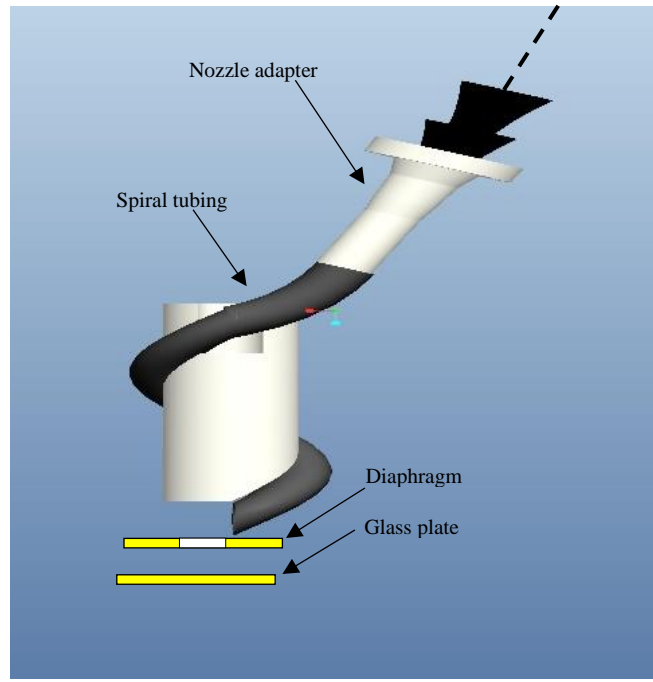
To simulate the spiral channel inside drill (Sanvik Coromat: Corodrill R840-0510-70-A1A), two 3D printed tool adapters were printed with ABS plastic and rigidly attached to the original nozzle of the MQL Unist system (Fig. 20). The inner channel surface of one adaptor was left in the as-printed condition, while the other was polished with acetone. A cotton bud was dipped in acetone and inserted in the internal diameter of the adaptor. The exit end of this adaptor was connected to a polyvinyl tubing wound around a helical adapter. The length of the adapter was 25.4 mm, and 25.4 mm pitch distance. This adapter simulated the helical profile of the inner passageways of the tool that carry the lubricant.

Our experiments included deposition of droplets on a glass slide giving us the information about the projected diameter of the droplets. The required aerodynamic diameter of the droplets could be determined by using the projected diameter and contact angle between the lubricant droplet and the glass slide. The contact angle between the lubricant and glass slide was determined for calculation of aerodynamic diameters.

To quantify the surface roughness of the printed nozzle, acetone was similarly wipe on the external surface of the 3D printed ABS adaptor. It was assumed that the smoothing effect would be the same whether acetone was applied on the outside or inside diameter of a nozzle. The Alicona Infinite Focus 3D digital microscope was used for surface characterization. Surface roughness was measured on 1.5 x 1.5 mm square at two different locations –polished and as-printed surfaces– on the external surface of the nozzle.



(a)



(b)

Figure 20 (a) Unist Micromist Lubrication System (b) Experimental setup for droplet collection

Experiments were performed near the optical microscope to ensure the sample droplets deposited on the slide were quickly moved to the microscope for analysis. Moving the samples over a large distance may have smeared the droplets giving inaccurate projected diameters thus affecting the calculation of droplet volumes. Furthermore, smaller droplets would have evaporated during transportation and affected accurate results.

The experimental set up is shown in Figure 20. Unist Micromist Lubrication system consisted of a flowmeter and pressure gauge to measure the flowrate and air pressure of compressed air. Coolube 2210 EP was introduced from the reservoir into the inner coaxial tube leading to the nozzle. The lubricant and compressed air mixed before the nozzle creating micromist that exited through the nozzle. The droplets passed through the nozzle adapter and spiral tubing and were deposited on the glass plate.

The UNIST Coolubricator system was used to generate the mist, and Coolube 2210 EP was used as the lubricant. Compressed air was controlled and measured with an Arrow B754FM air regulator. Droplets were collected through the following procedure.

1. A smooth glass plate (25 x 65 x 1 mm) was cleaned in alcohol then blew dried with compressed air.
2. It was placed horizontally approximately 3 mm below the vinyl tube to collect the oil droplets.

3. A thin paper diaphragm blocked the flow for approximately 30 seconds until visible oil droplets were seen, it was then quickly removed and reinserted within 10 s to allow sufficient number of droplets to form on the glass plate
4. Microdroplets were collected at air pressures of 275 kPa (40 psi), 415 kPa (60 psi) and 550 kPa (80 psi) with the frequency of pulse generator of MQL dispensing unit set to four cycles per second for the following combinations:
 - Case I. Formation of droplets exiting from the original coaxial nozzle of the Unist system ($\phi 1.58$ mm brass tube for oil, $\phi 2.55$ mm for air).
 - Case II. Formation of droplets exiting from the rough surface adaptor (as printed).
 - Case III. Formation of droplets exiting from the smooth surface adaptor (printed and polished).

The glass plate, containing freshly deposited microdroplets, were immediately placed under the Olympus STM6 microscope, from which high resolution image of microdroplets were captured in low intensity light to minimize the chance of evaporation of the tiny oil droplets. The pictures of the droplets were taken at six fixed positions on the glass slide for all the experiments. The images were then imported using ImageJ software, and then converted into binary 8-bit images for droplet analysis.

3.3 Droplet characterization using APS 3321

A parallel study to determine the droplet size distribution was done using Aerosol Particle Sizer (APS 3321). Original MQL nozzle and rough surface adapter were used to generate the droplets at inlet pressure of 550 kPa. The MQL nozzle was directed to the

inlet of the equipment and turned on for 5 seconds. The output of this APS System ranked droplet sizes that can be used for a distribution plot.

3.4 Micromilling

The workpieces to be machined were IN718 blocks having dimensions of 15 x 25 x 5 mm. They were additively manufactured using selective laser melting where 15 x 25 mm was the scanning XY plane and 5 mm was the building Z direction. The average diameter of the Inconel powder used was 50 μm . The printer used 160 W YAG laser to melt the powder to form the blocks. The blocks were stripe scanned with a hatching distance of 110 μm in Argon gas.

The blocks were clamped on their 20 mm length on the vice for machining. The blocks were face milled to ensure parallelism of the blocks to the XY-plane of the machine. A flat end mill of diameter 3.2 mm was used to remove 20 μm from the top to ensure the parallelism. After face milling the chips were blown away using compressed air. An uncoated square end micromill (Table 4) was used to perform the machining experiments.

Table 4 Micromilling tool (Adapted from "Performance Microtools", 2018)

Part No.	Cutter Diameter	End Shape	Helix Angle	Flute Length	No. of Flutes	Shank Diameter	Overall Length
TR-2-0100-S	0.254 mm	Square End	30°	0.762 mm	2	3.175 mm	38.1 mm

The microtool was mounted into the collet of the milling machine and tool positioning

was performed to zero out the X, Y and Z axis offsets using the following procedure.

1. The table was moved in X and Y direction to bring the block directly below the tool.
2. The terminals of the digital multimeter were connected to the shank of the tool and the workpiece. It measured the change in resistivity one the tool came in contact with the workpiece and the circuit was closed.
3. The tool was moved down slowly using Hand Jog until it made contact with the workpiece. Slow motion ensured that the tool was stopped when the multimeter beeped due the change in resistivity caused by the tool coming in contact with the workpiece.
4. The value of Z was highlighted in G54 line in the “Work Zero Offset” menu located on the display interface of HAAS OM2 CNC milling machine. The current position of the tool was recorded as the coordinate origin for Z axis by pressing the “Part Zero Set” button.
5. The tool offsets for X and Y axes were determined using the same method. After pressing “Part Zero Set” to record the position of the tool, the radius of the tool was added to the value in G54 using the numeric keypad as the center of the tool was located on the left of the workpiece for X axis and at the bottom of the workpiece for Y axis.

The outlet of the polyvinyl tubing wrapped around the helical adapter was kept at 3 mm from the tool workpiece interface. A two level factorial experimentation was performed. A total of eight experiments were performed (Table 5). The

experiments were done using the as printed and polished nozzle adapters. Each nozzle adapter was used to generate droplets at the pressures of 275 kPa and 550 kPa. The cutting speed, chipload and depth of cut being kept constant (Table 6). Two repetitions were done for each condition to ensure repeatability.

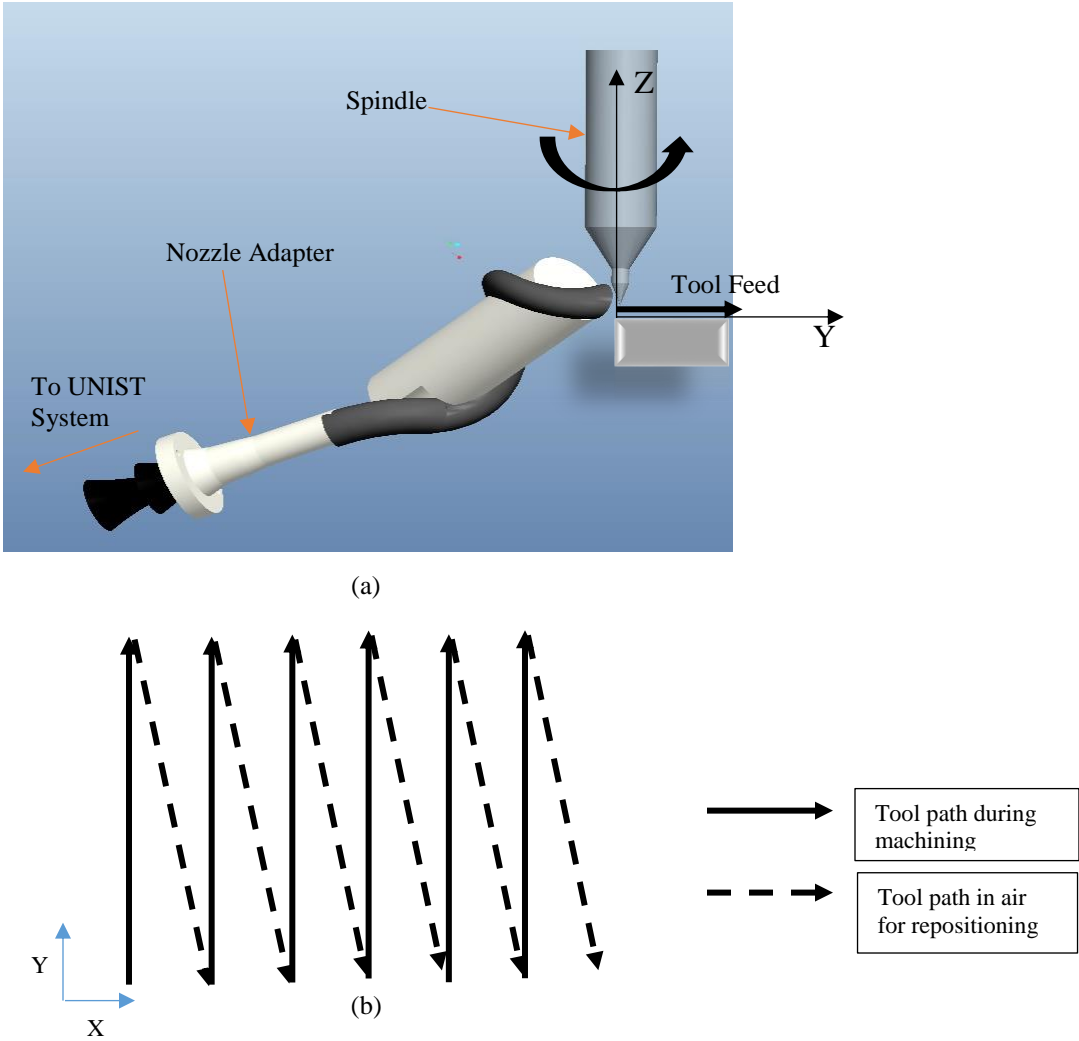
Table 5 Experimental iterations

Experiment Number	Nozzle	Pressure (kPa)
1	rough	550
2	rough	275
3	rough	275
4	rough	550
5	smooth	550
6	smooth	275
7	smooth	275
8	smooth	550

Table 6 Machining parameters

Chipload ($\mu\text{m}/\text{tooth}$)	1.8
Cutting Speed (m/min)	13.6
Feedrate (mm/min)	40
Depth of Cut (μm)	20
Number of Slots Milled (No.)	10

After milling, a block was ultrasonically cleaned in 70% iso-propyl alcohol for 5 minutes and then blew-dry using compressed air to get rid of the chips, lubricant oil and dirt on the workpiece.



3.5 Metrology

Profile roughness R_a , surface roughness S_a and slot width of milled blocks were measured using the Alicona Infinite Focus digital microscope. A 5X objective lens was used to capture images of the milled slots. Due to the large size of the area to be measured, “General Image Field” option on Alicona was used. The images were captured in the following way.

1. The objective lens were moved to the top right of the block and the top surface of the block was brought into focus.
2. The objective lens was zoomed out until the image was out of focus. The “Add Position” option on the software interface was selected to store this region in the software’s memory.
3. The objective lens was moved to the top left region of the machined block and image was added to the memory of the software.
4. The worktable was moved such that the objective lens were at the bottom left corner of the workpiece and the objective lens were zoomed in until the workpiece came in focus and then went out of focus again and the image was added into the memory of software by clicking on “Add Position”.
5. The worktable was moved until the objective lens were at the bottom right corner of the workpiece and this position was added into the software’s memory as well.
6. “Start Measurement” was selected on the software interface. The software stitched together all the images collected and displayed the high definition image.

This image was then imported into Profile Roughness and Surface Roughness module for required measurements.

Surface finish calibration was done using the known $2.95 \mu\text{m}$ Ra surface standard (Mitutoyo, code No. 178-602). The optimal profile length was chosen to be $500 \mu\text{m}$.

Surface roughness was measured inside a $150 \times 500 \mu\text{m}$ rectangular region position at center of a milled slot. Two measurements were performed within 1 mm of the start of each slot as the tool wear was the least at start of the slots. Slot widths were measured at the end of the slots and then subtracted from the initial diameter of the milling tool to determine tool wear.

2-D Image Measurement module of Alicona InfiniteFocus microscope was used to measure the slot widths. The caliper function in the module was used to measure the width of the slot. The readings were taken twice and the results were averaged out to obtain the width of the slot.

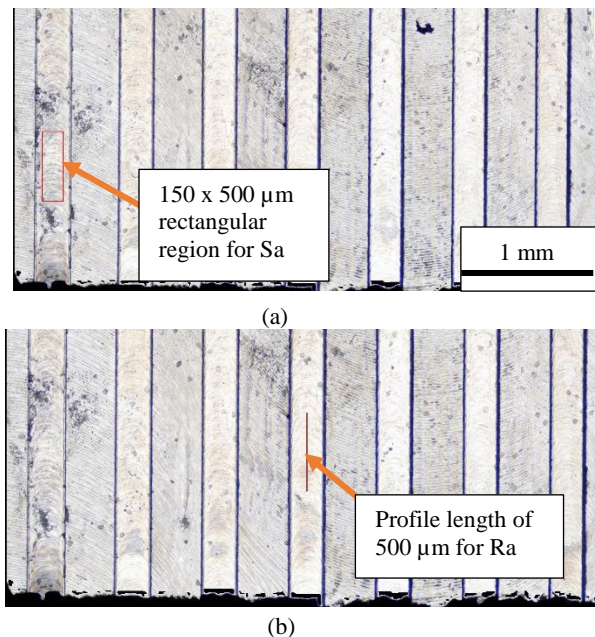


Figure 22 (a) Measurement of Surface Roughness (b) Measurement of Profile Roughness

3.6 Air flow velocity

The flow velocity of compressed air and MQL after passing through the rough and smooth nozzle adapters was measured using an $\text{\O} 1$ mm probe of Kanomax Climomaster 6501 anemometer into the flow stream of micromist. The experiments were conducted at input pressures of 275 kPa and 550 kPa. The anemometer probe was rigidly attached to the vice on the worktable of HAAS OM 2 CNC Milling Machine. The MQL nozzle was mounted on the side wall of the CNC milling machine and the nozzle was positioned perpendicular to the anemometer probe. A NC program was used to move the anemometer along the path shown in Figure 23. 17 readings were taken at an interval of 0.5 cm in the Y direction before the anemometer moved 1 cm away from the nozzle in X direction. The probe paused at each interval for five seconds to record the reading. After measuring the flow velocity of MQL, the system was purged from lubricant by emptying the tank and allowing the system to run for 2 hours. An absorbent paper was placed in front of the nozzle to ensure that no lubricant oil remained in the system. The experiments were repeated to measure the flow velocity of compressed air.

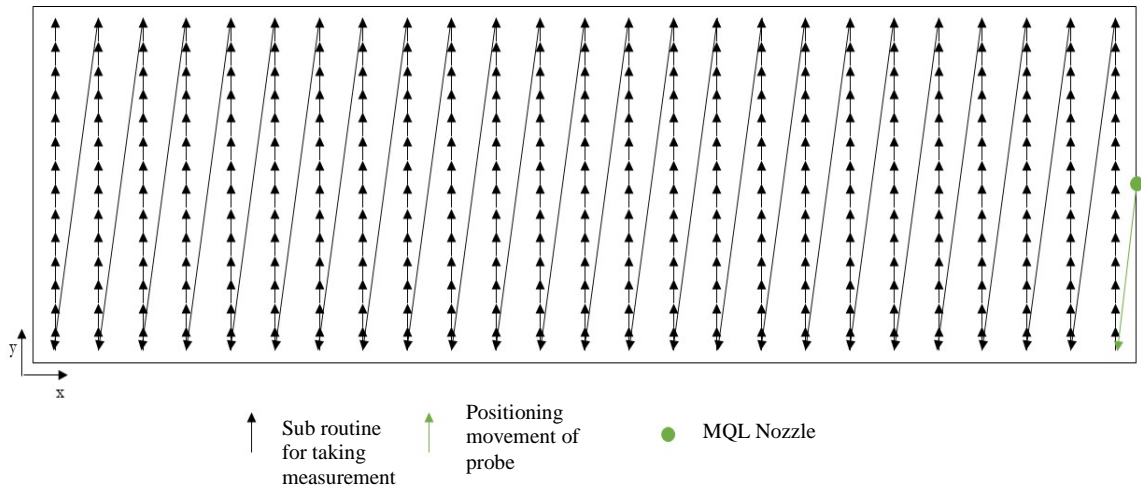


Figure 23 Moving path of anemometer probe

4. RESULTS AND DISCUSSION

Table 7 shows the calibration results to determine the profile length to measure profile roughness (R_a). $L_c = 2500 \mu\text{m}$ gave the minimum error, therefore all measurements used this value of L_c along with a profile length of $500 \mu\text{m}$ to measure R_a .

Table 7 R_a Calibration Results using Mitutoyo Surface Standard $R_a = 2.95 \mu\text{m}$

Profile Length (μm)	L_c (μm)	Line Roughness, R_a (μm)	% Error
100	800	1.25	57.7
150	800	1.44	51.2
200	800	1.40	52.5
300	800	1.34	54.5
400	800	1.51	48.8
500	2500	2.85	3.3
600	800	1.92	35.0

The surface roughness S_a of the as-printed (rough) and acetone polished (smooth) nozzles were measured to be $16.8 \mu\text{m}$ and $3.2 \mu\text{m}$ respectively. Since the internal flow of micromist inside a $\phi 3 \text{ mm}$ nozzle affected by its surface finish, it is expected that the mist flow –either laminar or turbulent–would affect the resulting droplets.

4.1 Contact Angle

The caliper function in the Olympus STM 6 microscope's software was used to measure the projected diameters of the droplets. The projected diameters for five drops of each volume are shown in Table 8.

Table 8 Projected diameters and contact angles for 5 samples at 0.2 μL and 0.3 μL volumes of Coolube 2201 EP on glass

Volume	0.3 μL	0.2 μL
Projected Diameter (μm)	1764.72	1568.64
	1687.32	1537.68
	1754.40	1640.88
	1733.76	1553.16
	1800.84	1651.20
Avg. Dia. (μm)	1748.21	1590.31
θ°	30.7	28.0

Assuming spherical shape of a small droplet on a flat and smooth surface, the contact angle can be shown relating to drop size and droplet volume using equations (3) and (4).

The projected diameter along with the measured volume was plugged in equation (3) to determine the contact angle between Coolube 2210 EP and glass slide used to collect the droplets. Table 8 summarizes the results of contact angle calculations for Coolube 2210EP on glass when a known volume of lubricant was measured with a micropipette. The average value was calculated to be 29.3° . The value of contact angle was then used in equations (3-4) to calculate the airborne diameters of droplets.

4.2 Air Flow Velocity

The velocity maps of compressed air exiting the rough and smooth nozzle adapters at inlet pressure of 275 kPa and 550 kPa are shown in Figures 24 (a,b).

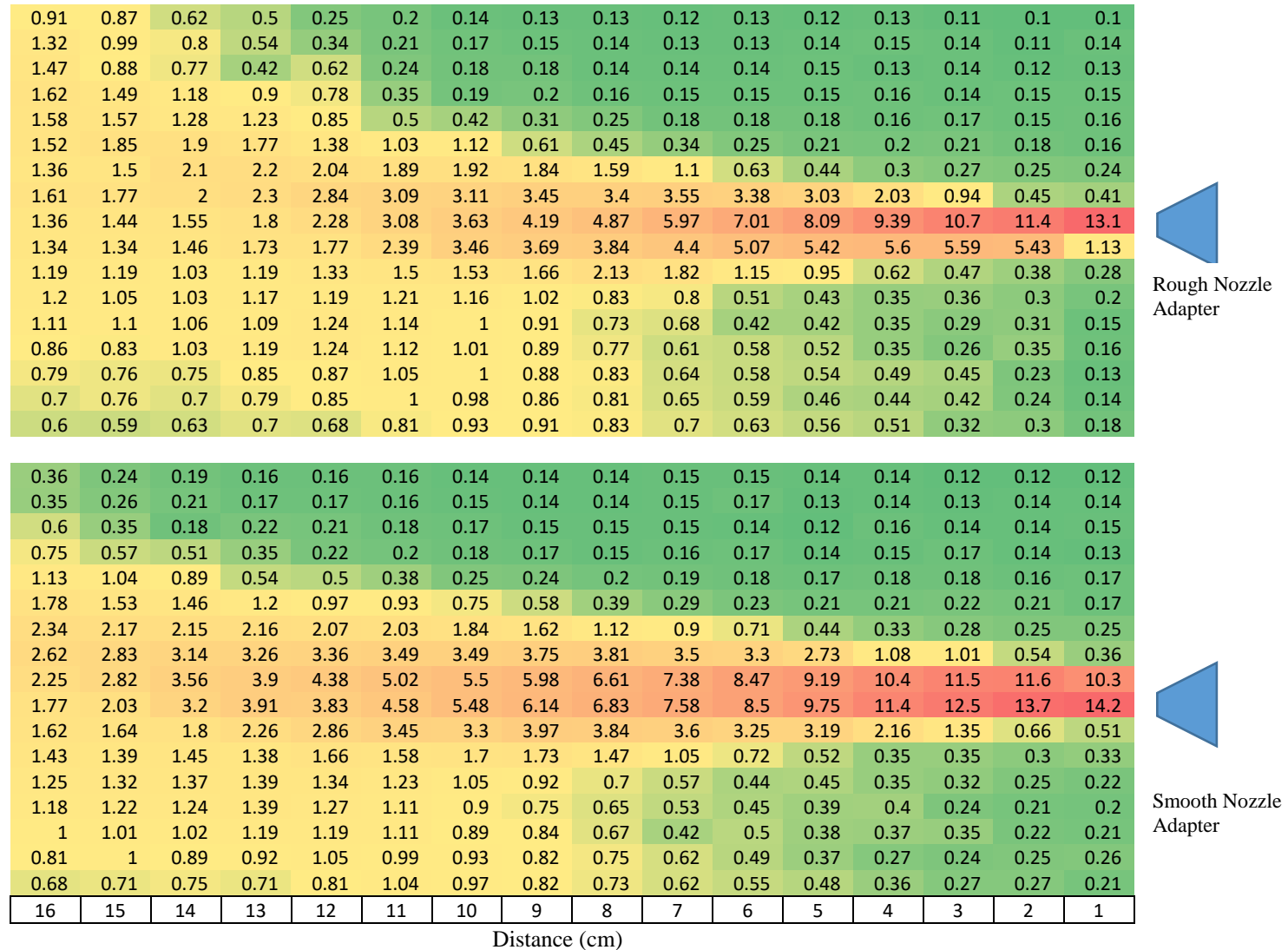


Figure 24 (a) Exit air velocity (m/s) at 550 kPa for rough nozzle adapter and smooth nozzle adapter (b) Exit air velocity (m/s) at 275 kPa for rough nozzle adapter and smooth nozzle adapter

0.9	0.92	0.43	0.45	0.31	0.21	0.21	0.18	0.14	0.15	0.14	0.12	0.11	0.12	0.12	0.11
1.04	0.95	0.61	0.5	0.3	0.2	0.29	0.21	0.13	0.14	0.12	0.12	0.11	0.13	0.1	0.12
1.15	1.21	0.66	0.49	0.36	0.3	0.23	0.16	0.15	0.15	0.13	0.13	0.13	0.13	0.13	0.13
1.01	1.31	0.93	0.63	0.51	0.5	0.28	0.2	0.16	0.16	0.13	0.13	0.14	0.13	0.15	0.13
1.25	1.39	1.29	1.13	0.55	0.34	0.35	0.24	0.19	0.18	0.16	0.14	0.15	0.14	0.13	0.15
1.33	1.4	1.47	1.04	0.65	0.88	0.62	0.66	0.35	0.26	0.21	0.19	0.16	0.16	0.16	0.16
1.39	1.51	1.54	1.54	1.25	1.56	1.3	1.1	1.03	0.8	0.6	0.42	0.28	0.21	0.22	0.18
1.51	1.38	1.38	1.58	1.89	2.09	2.08	2.14	2.33	2.52	2.29	2.21	1.77	1.13	0.53	0.33
1.27	1.38	1.42	1.61	2	2.37	2.61	3.15	3.64	4.44	5.24	6.2	7.09	8.68	9.88	11.2
1.26	1.29	1.28	1.14	1.28	2.01	2.25	2.72	3.29	3.54	3.69	4.91	4.8	5.01	4.06	2.02
1.17	1.23	1.22	1.18	1.2	1.23	1.58	1.84	1.53	1.52	1.3	1.01	0.74	0.41	0.3	0.28
1.12	1.09	1.18	1.24	1.22	1.13	1.08	0.97	0.79	0.62	0.53	0.35	0.28	0.3	0.23	0.23
1.1	1.05	1.13	1.3	1.21	1.12	0.99	0.81	0.67	0.52	0.5	0.38	0.35	0.26	0.27	0.17
0.93	1	1.05	1.09	1.18	1.1	0.93	0.78	0.61	0.47	0.33	0.39	0.31	0.24	0.22	0.18
0.83	0.91	0.92	1.07	1.1	1.09	0.95	0.84	0.69	0.59	0.35	0.34	0.43	0.28	0.2	0.2
0.74	0.75	0.85	0.85	1.04	1.12	0.98	0.92	0.8	0.69	0.56	0.48	0.38	0.19	0.33	0.21
0.63	0.65	0.74	0.79	0.82	0.92	0.94	0.88	0.74	0.64	0.56	0.43	0.45	0.3	0.28	0.35



Rough Nozzle Adapter

0.72	0.91	0.9	0.93	0.73	0.46	0.24	0.21	0.18	0.14	0.12	0.1	0.12	0.1	0.1	0.11
0.8	0.88	1	0.77	0.9	0.43	0.42	0.22	0.21	0.16	0.12	0.11	0.12	0.1	0.1	0.09
0.93	1	1.08	1.01	0.85	0.39	0.34	0.33	0.29	0.15	0.12	0.12	0.12	0.1	0.11	0.09
1	1.1	1.12	1.07	0.71	0.52	0.52	0.42	0.21	0.16	0.12	0.14	0.13	0.11	0.11	0.13
1.13	1.12	1.21	1.26	0.86	0.66	0.5	0.4	0.33	0.2	0.15	0.15	0.13	0.11	0.12	0.14
1.28	1.25	1.15	1.29	1.26	1.06	0.98	0.54	0.56	0.3	0.19	0.18	0.15	0.17	0.15	0.15
1.28	1.28	1.21	1.36	1.55	1.5	1.63	1.28	0.98	0.7	0.57	0.47	0.3	0.2	0.2	0.2
1.2	1.26	1.17	1.34	1.65	1.78	1.8	2.01	2.01	1.95	2.1	2.03	1.7	1.3	0.8	0.39
1.14	1.3	1.18	1.09	1.4	1.9	2.4	2.45	2.79	3.24	4	4.56	5.87	7.35	9.62	11.6
1.02	1.2	1.16	1.06	1.1	1.44	1.8	1.88	2.2	2.21	2.86	3.21	3.5	3.85	3.54	2.26
0.89	1.08	1.15	1.06	1.1	1.08	1.12	1.23	1.19	1.15	1.08	0.91	0.63	0.4	0.45	0.39
0.95	1.06	1.11	1.19	1.13	1.1	1.02	0.92	0.82	0.8	0.61	0.45	0.32	0.23	0.32	0.28
0.9	0.92	0.98	1.14	1.15	1.04	0.99	0.85	0.75	0.6	0.52	0.43	0.28	0.34	0.27	0.21
0.81	0.86	0.84	0.99	0.95	1.1	0.98	0.9	0.64	0.73	0.6	0.45	0.34	0.42	0.28	0.29
0.71	0.63	0.86	0.98	0.98	0.99	0.95	0.88	0.86	0.64	0.55	0.41	0.45	0.33	0.26	0.35
0.56	0.57	0.64	0.79	0.89	1.05	0.94	0.92	0.78	0.61	0.68	0.49	0.45	0.34	0.35	0.38
0.48	0.45	0.51	0.6	0.7	0.85	0.94	0.87	0.8	0.75	0.57	0.5	0.57	0.52	0.42	0.3



Smooth Nozzle Adapter

16	15	14	13	12	11	10	9	8	7	6	5	4	3	2	1
----	----	----	----	----	----	----	---	---	---	---	---	---	---	---	---

Distance (cm)
Figure 24 Continued

At 550 kPa (Fig. 24), the velocities measured for compressed air passing through the rough nozzle adapter were lower than those measured with the use of smooth nozzle. The maximum velocity at 1 cm away from the tip, measured with the use of rough nozzle, was 13.1 m/s compared to 14.2 m/s measured using the smooth nozzle. The increased surface roughness of the nozzle restricted the flow of compressed air resulting in lower velocities. Along the axis of the nozzle, the flow velocity dropped to 3 m/s at a distance of 11 cm from the nozzle with the use of rough nozzle. This distance increased to approximately 14 cm when the polished nozzle was used. At 275 kPa air pressure (Fig. 24 a and b), the maximum flow velocities reduced for both rough and smooth nozzle. The maximum velocity measured was 11.2 m/s for rough nozzle adapter and 11.6 m/s for smooth adapter. At low pressure, the flow velocities reduced to 3 m/s at 9 cm from the rough nozzle and 7 cm from the smooth nozzle. These distances were lower than those measured at 550 kPa as lower pressure at the inlet generated lower air velocities.

The velocity maps of MQL droplets exiting through rough and polished nozzle adapters are shown in Figure 27 (a,b).

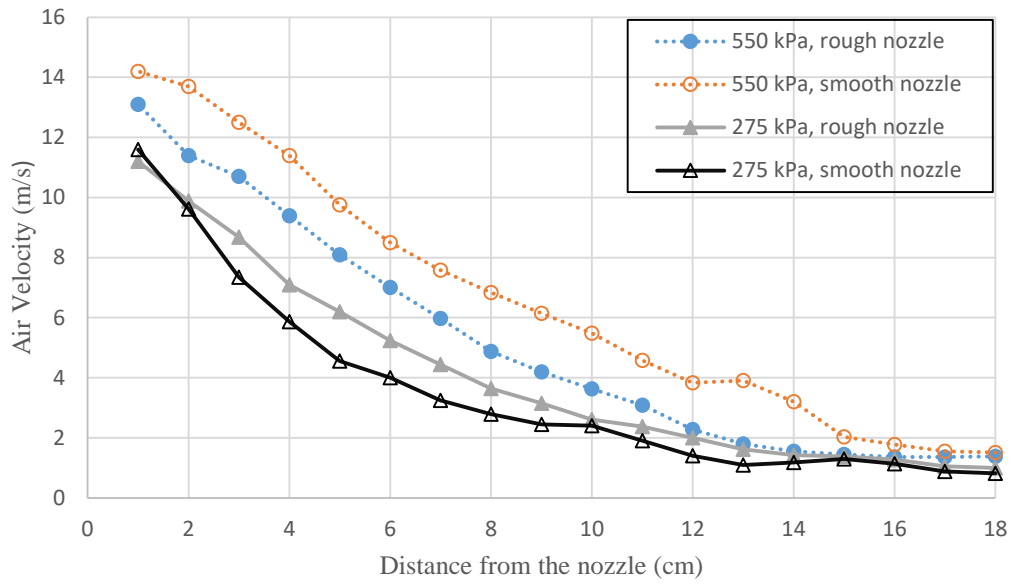


Figure 25 Air flow velocity along nozzle axis

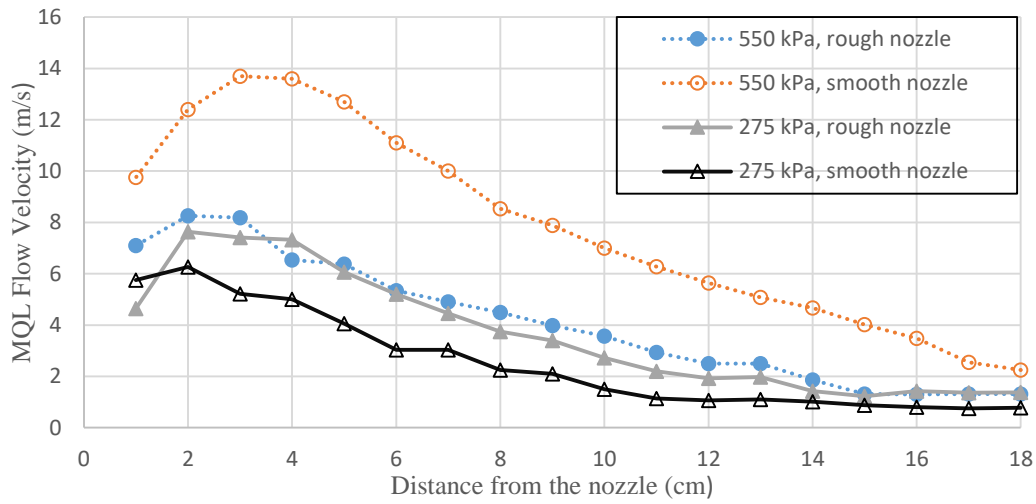


Figure 26 MQL flow (air + lubricant) velocity along the nozzle axis

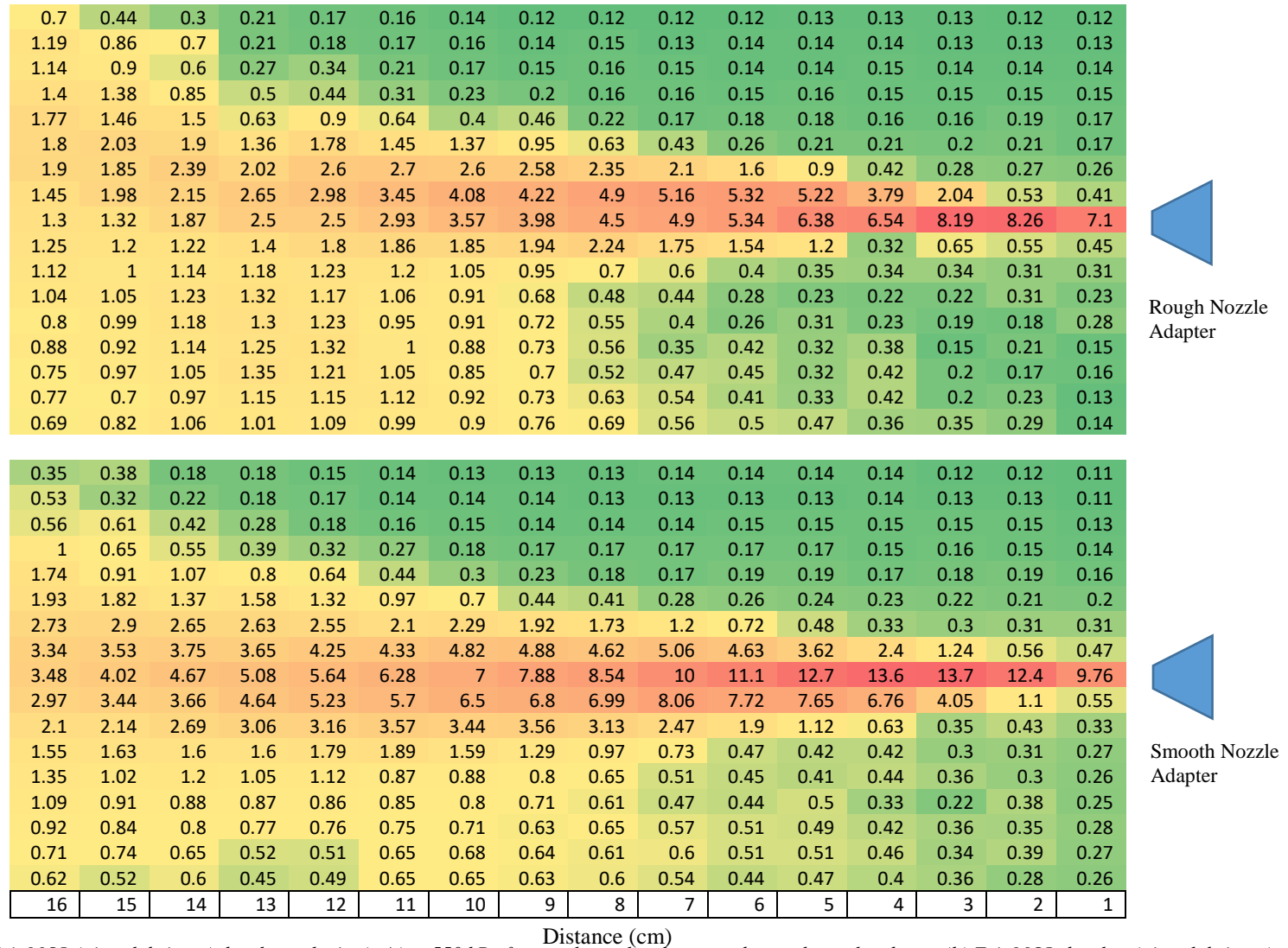


Figure 27 (a) Exit MQL (air + lubricant) droplets velocity (m/s) at 550 kPa for rough nozzle adapter and smooth nozzle adapter (b) Exit MQL droplets (air + lubricant) velocity (m/s) at 275 kPa for rough nozzle adapter and smooth nozzle adapter

0.98	0.78	0.7	0.3	0.23	0.24	0.15	0.13	0.13	0.12	0.11	0.13	0.13	0.12	0.12	0.1
1	1.15	0.93	0.4	0.6	0.17	0.15	0.15	0.15	0.13	0.13	0.12	0.12	0.13	0.11	0.11
1.11	1.08	0.87	0.43	0.56	0.2	0.16	0.16	0.16	0.13	0.12	0.13	0.13	0.14	0.14	0.11
1.17	1.23	0.75	0.48	0.5	0.21	0.18	0.16	0.19	0.14	0.13	0.13	0.13	0.12	0.13	0.12
1.17	1.38	0.85	0.75	0.45	0.46	0.33	0.17	0.2	0.14	0.14	0.13	0.13	0.14	0.13	0.13
1.26	1.33	1.01	1.02	0.86	0.5	0.4	0.22	0.19	0.17	0.16	0.14	0.15	0.16	0.15	0.14
1.35	1.33	1.37	1.42	0.96	0.95	0.55	0.47	0.3	0.27	0.2	0.2	0.17	0.18	0.18	0.15
1.46	1.57	1.43	1.6	1.54	1.23	1.25	1.29	0.83	0.66	0.58	0.37	0.21	0.2	0.2	0.2
1.4	1.3	1.63	2	2.03	2.24	2.29	2.4	2.29	2.62	2.34	2.04	1.45	0.72	0.36	0.24
1.43	1.23	1.43	1.97	1.93	2.2	2.72	3.4	3.75	4.46	5.21	6.06	7.33	7.41	7.64	4.64
1.33	1.26	1.05	1.25	1.9	2.08	2.03	3.2	3.36	3.45	3.54	3.95	4.36	3.76	3	1.16
1.13	1.12	1.1	1.05	1.13	1.29	1.34	1.35	1.23	1.29	1.01	0.75	0.53	0.27	0.27	0.25
1.02	1.03	1.11	1.09	1.16	1.08	1.01	0.92	0.77	0.6	0.43	0.23	0.23	0.29	0.2	0.21
0.88	0.83	1.17	1.31	1.25	1.1	0.95	0.73	0.63	0.43	0.36	0.21	0.18	0.19	0.19	0.16
0.87	0.92	1.12	1.3	1.31	1.1	0.82	0.67	0.63	0.4	0.35	0.28	0.21	0.22	0.27	0.16
0.74	0.76	0.98	0.94	1.3	1.15	0.91	0.78	0.46	0.42	0.35	0.48	0.33	0.25	0.25	0.26
0.63	0.74	0.61	1	0.95	1.02	0.91	0.77	0.55	0.63	0.43	0.44	0.46	0.25	0.22	0.16
0.68	0.7	0.9	0.88	0.73	0.52	0.49	0.22	0.15	0.15	0.12	0.13	0.1	0.11	0.1	0.1
0.63	0.88	0.95	0.92	0.85	0.6	0.45	0.3	0.23	0.18	0.13	0.14	0.13	0.12	0.09	0.08
0.84	0.9	1.05	1.03	0.9	0.78	0.63	0.35	0.26	0.22	0.15	0.13	0.11	0.11	0.11	0.1
0.9	1.06	1.05	0.98	0.9	0.65	0.52	0.45	0.32	0.2	0.16	0.12	0.15	0.12	0.11	0.1
0.8	1.1	1.11	1.13	1.05	0.95	0.85	0.55	0.4	0.3	0.17	0.15	0.13	0.13	0.11	0.12
1.05	1	1.19	1.11	1.17	1.2	0.9	0.8	0.57	0.44	0.17	0.19	0.13	0.13	0.12	0.14
0.9	1.17	1.05	1.02	1.03	1.12	1.33	0.9	0.44	0.53	0.28	0.22	0.15	0.13	0.15	0.13
0.83	1.09	1.12	1.06	1.14	1.22	1.45	1.27	1	0.8	0.7	0.35	0.22	0.21	0.17	0.18
0.84	0.78	1	1.06	1.24	1.27	1.66	1.78	1.7	1.73	1.51	1.68	1.15	0.62	0.36	0.25
0.8	0.88	1.01	1.1	1.06	1.14	1.5	2.1	2.25	3.03	3.03	4.06	5	5.22	6.26	5.75
0.65	0.81	0.96	1.04	0.95	1.05	1.32	1.35	1.06	2.38	2.66	2.98	3.51	2.8	2.3	1.29
0.8	0.6	0.9	1	0.98	1.16	1.03	1.04	0.89	1.18	1.04	0.88	0.65	0.41	0.37	0.36
0.69	0.72	0.86	1	0.99	1	1.02	0.95	0.85	0.75	0.63	0.47	0.47	0.32	0.24	0.21
0.6	0.6	0.76	1.14	0.95	1.07	0.95	0.92	0.81	0.73	0.66	0.44	0.33	0.45	0.32	0.23
0.58	0.66	0.81	0.9	1.1	1.06	0.98	0.9	0.82	0.63	0.6	0.45	0.47	0.37	0.33	0.32
0.4	0.49	0.63	0.95	1.01	0.95	0.9	0.9	0.8	0.7	0.62	0.5	0.44	0.35	0.44	0.2
0.44	0.37	0.55	0.69	0.79	0.87	0.95	0.8	0.83	0.61	0.68	0.58	0.49	0.3	0.4	0.42
16	15	14	13	12	11	10	9	8	7	6	5	4	3	2	1



Rough Nozzle Adapter



Smooth Nozzle Adapter

Distance (cm)

Figure 27 Continued

The maximum velocity of the droplets measured with the use of rough nozzle was 8.26 m/s. It was lower than the maximum velocity of the droplets exiting the smooth nozzle. After travelling 10 cm, the velocity of droplets exiting the rough nozzle had decreased to 3.57 m/s compared to 7 m/s of the droplets exiting the smooth nozzle. At pressure of 275 kPa, the trend observed in velocities was reversed. Droplets exiting the rough nozzle adapter had a higher velocity of 7.64 m/s compared to the velocity of 6.26 m/s measured for the droplets exiting the smooth nozzle. This reversal may be due to the large droplet size generated at 275 kPa using the polished nozzle adapter (Table 9). Larger droplets would have lower velocities due to their high mass and inertia dampening the effect of high pressure on the speed of droplets.

Li et al. (2015) used the original nozzle to measure the air flow velocities at 200 kPa and 600 kPa. They measured the air flow velocities greater than 35 m/s along the central profile for 9 cm at 200 kPa and 14 cm at 600 kPa. We observed that the maximum air flow velocities decreased due to constricted flow in the nozzle adapters as shown in Figure 25. The maximum air flow of velocity 14.2 m/s was observed with the use of smooth nozzle adapter at 550 kPa.

4.3 Droplet Characterization

Typical trends of size and distribution of droplets captured using the Olympus STM 6 microscope documented along with the type on nozzle and pressure variation are shown in Figure 28.

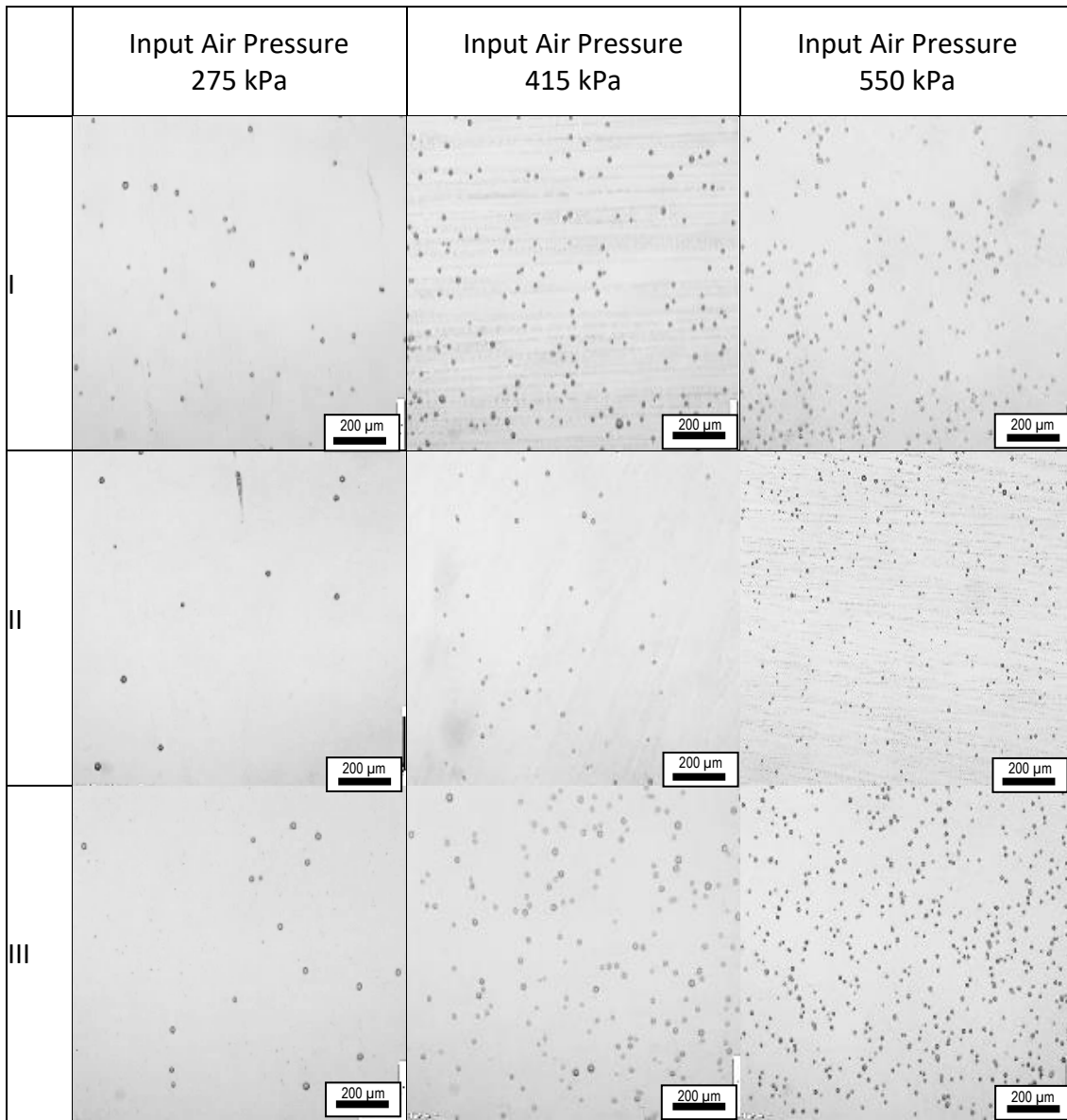
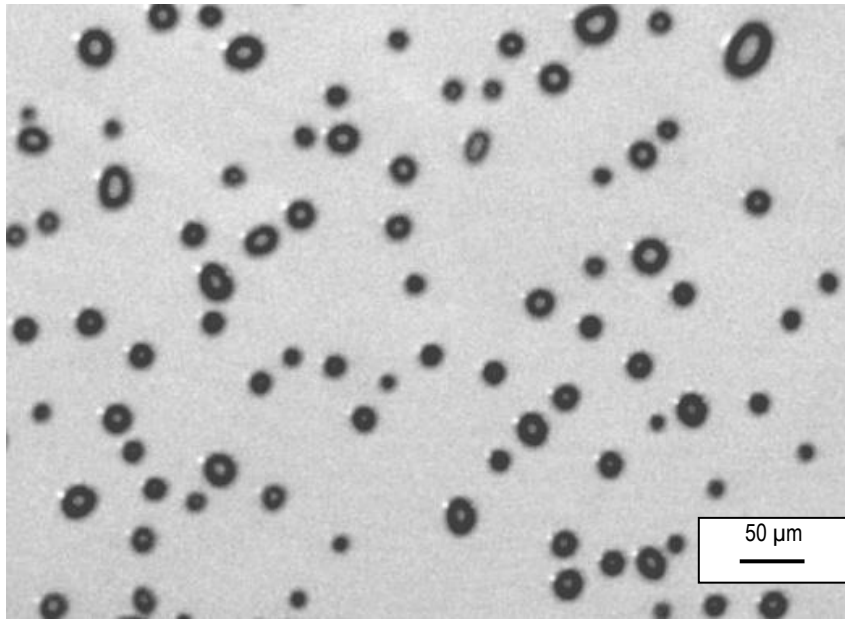
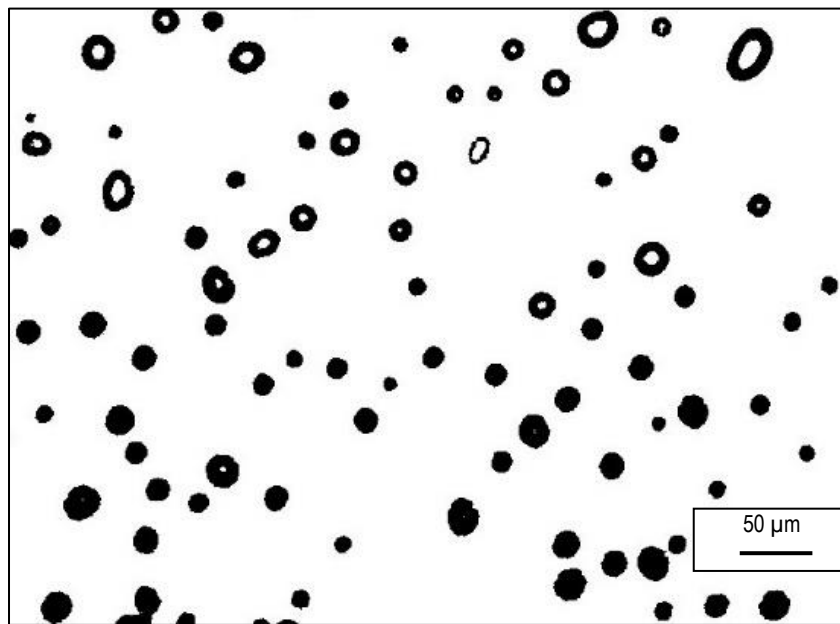


Figure 28 Resulting microdroplet images with (I) from original nozzle, (II) rough nozzle, and (III) smooth nozzle

The images were then converted to bitmap images using ImageJ. Figure 29 shows typical images of microdroplets before and after binary transformation.



(a)



(b)

Figure 29 . Micro droplet images for sample collected at 550 kPa using the original nozzle (a) as deposited on glass, (b) after bitmap conversion.

ImageJ gave the number and projected area of the droplets on the glass slide. The droplets were assumed to be perfect circles and their projected diameter was extracted using the formula for the area of the circle.

$$P = \left(\frac{4A}{\pi}\right)^{\frac{1}{2}} \quad (5)$$

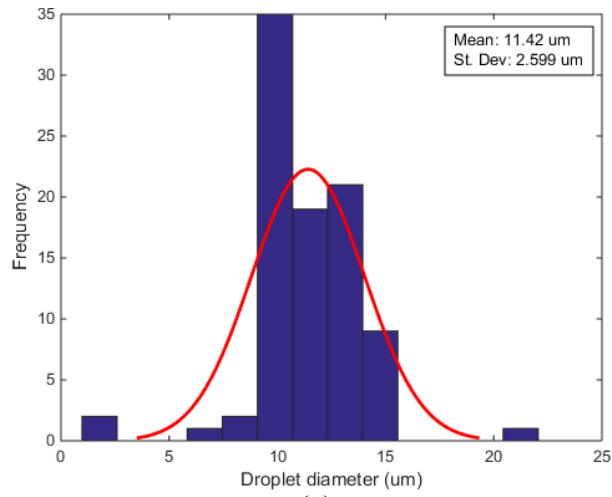
Where

P : Projected diameter of the droplet (μm)

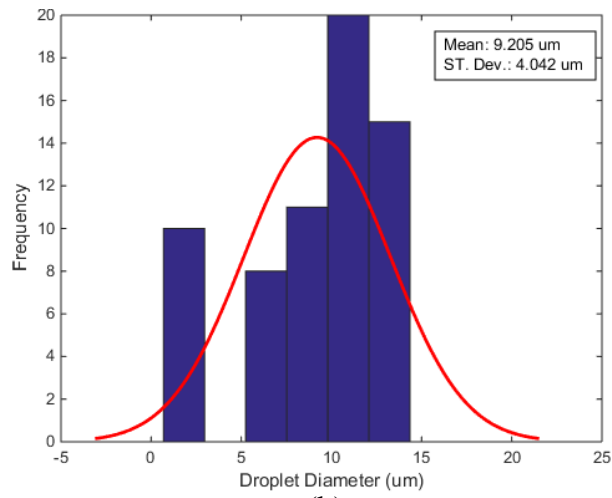
A : Projected area of the droplet (μm^2)

The projected diameter of the droplet was used along with the contact angle of 29.3° and equations (3) and (4) to determine the airborne diameter of the droplets.

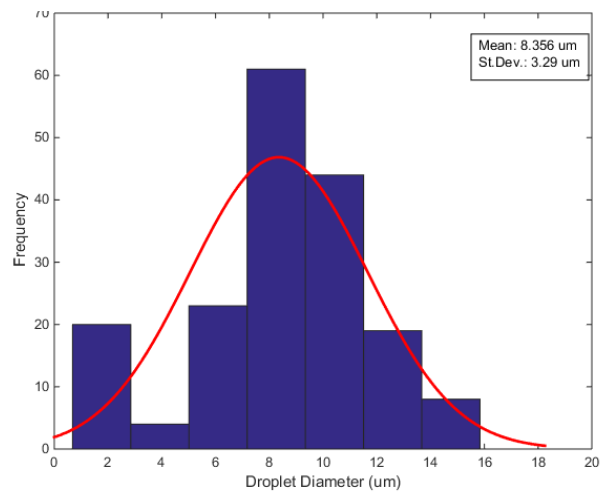
The distributions of the droplets were plotted using MATLAB. Fig. 28 documents the droplet distributions and sizes depending on the respective nozzles and air pressures. There were very small droplets ($< 0.5 \mu\text{m}$) that were not captured during image conversion using ImageJ software. There are also few larger droplets due to unavoidable coalescence of smaller droplets as shown in Fig. 29. High pressure breaks down oil droplets into many smaller ones as evidence with high density droplet on the last column (highest pressure of 550 kPa) of Fig. 28. As we move across the columns in Figure 28 indicating the increase in pressure, we observe the fact the size of droplets become smaller with the number of droplets increasing. As the smaller droplets have a lower settling velocity, all of them didn't get deposited on the glass slides and the actual number exiting the nozzle would be even higher at higher pressures. A more quantitative analysis of the droplet size and distribution can be done by looking at the droplet distributions in Figures 30, 31 and 32.



(a)

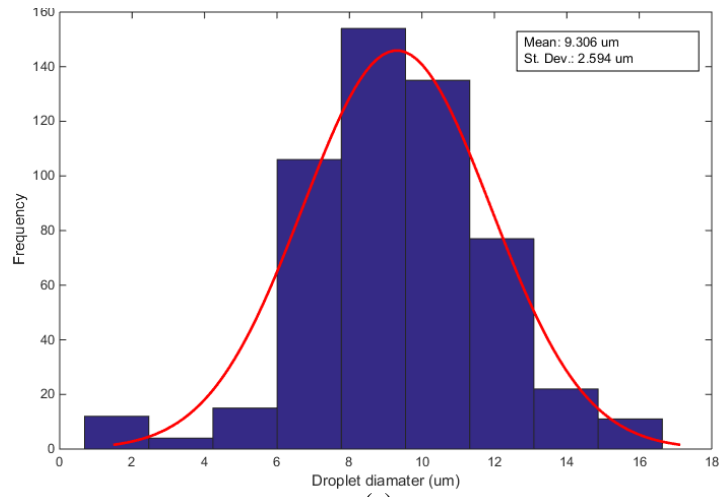


(b)

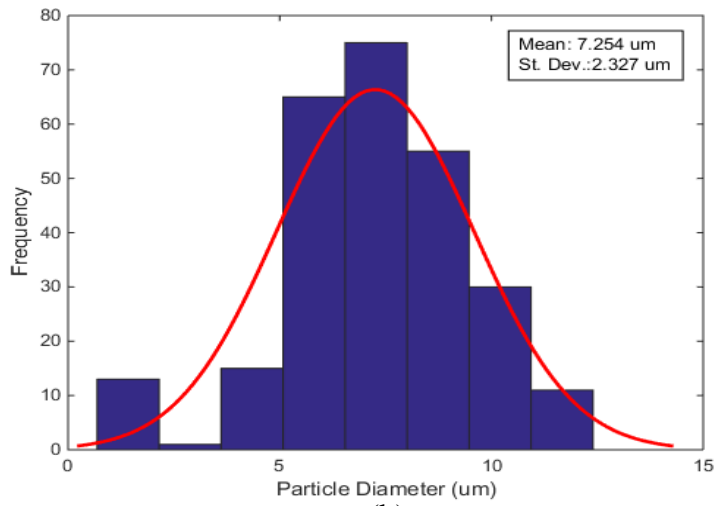


(c)

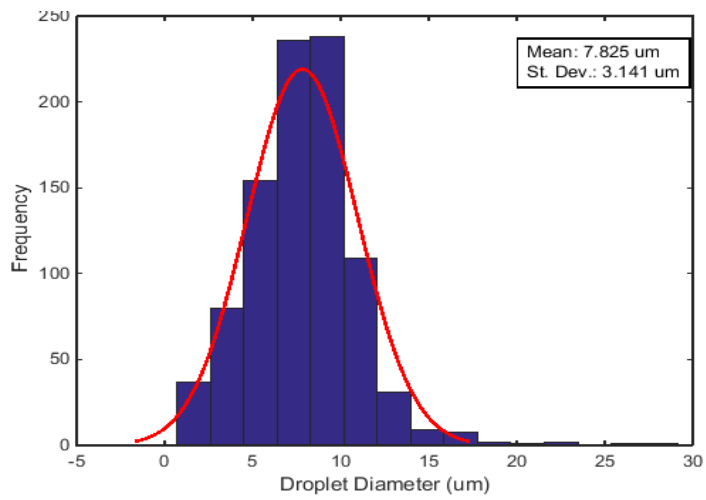
Figure 30 Droplet distribution at 276 kPa with (a) with smooth nozzle (b) with rough nozzle (c) original nozzle



(a)

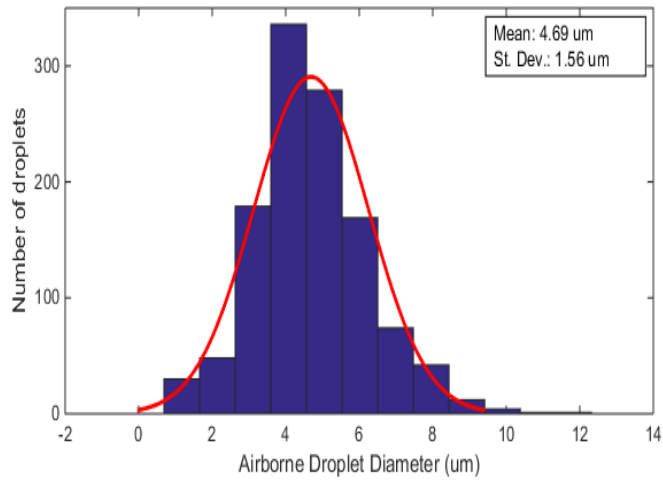


(b)

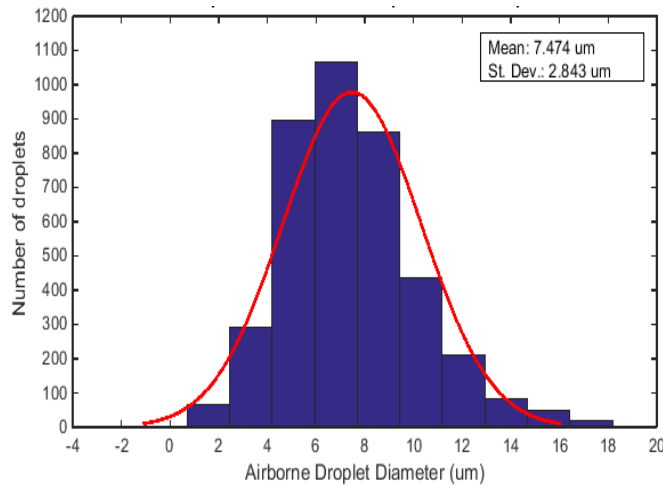


(c)

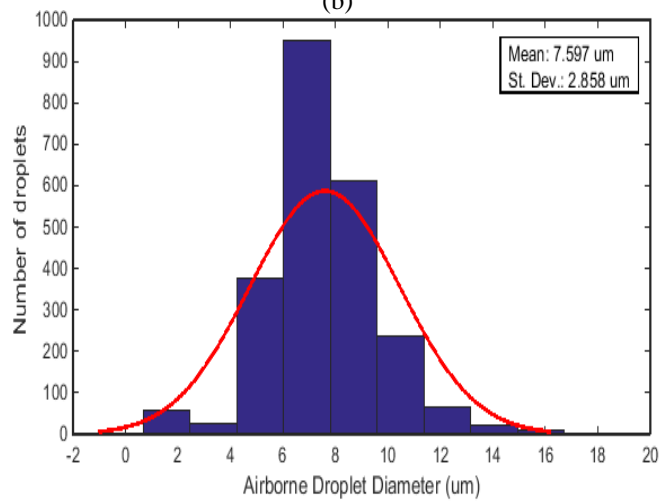
Figure 31 Droplet distribution at 415 kPa with (a) with smooth nozzle (b) with rough nozzle (c) original nozzle



(a)



(b)



(c)

Figure 32 Droplet distribution at 550 kPa with (a) with rough nozzle (b) with original nozzle (c) smooth nozzle

The histogram bar widths for the histogram were determined by the following relation (Scott, 1979).

$$W = 3.49\sigma N^{-\frac{1}{3}} \quad (6)$$

Where

σ : Standard deviation

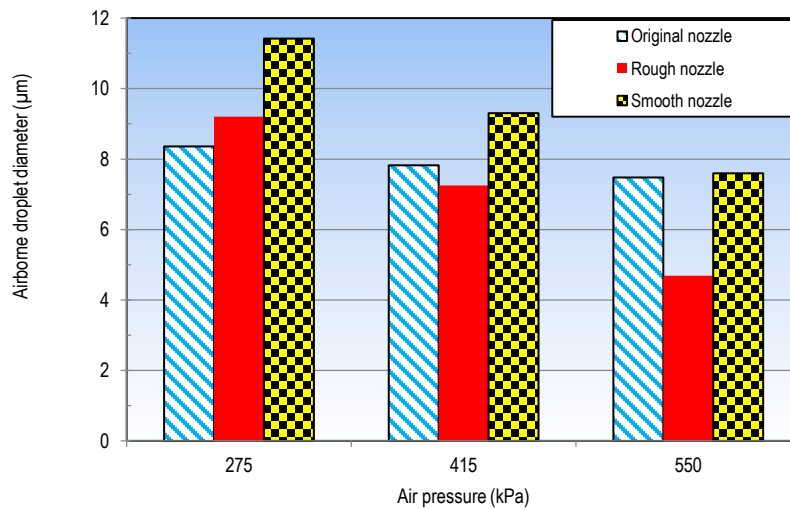
N : Number of droplets

W : Width of the histogram bar

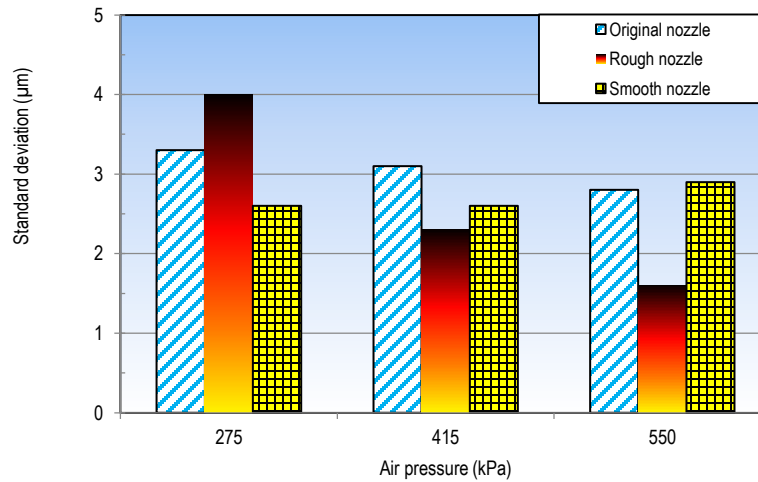
The droplets seemed to follow a normal distribution. The peaks in the left most histogram bars of Figure 30 may be attributed to splattering of a larger droplets that created several smaller droplets. This observation is consistent with the fact that the largest droplets were formed at the lowest pressure of 276 kPa and the chances of splattering on impact were high. The lowest MQL flow velocity of 5.75 m/s was observed at this configuration due to formation of larger droplets of lubricant. Larger droplets having higher inertia reduced the speed of the droplets. These peaks disappear when the pressure is increased resulting in higher air velocity (Figure 24). They are non-existent in the distribution of lubricant droplets at the highest pressure of 550 kPa. The high pressure produced smaller droplets which didn't splatter on striking the glass slide. Table 9 shows the mean and standard deviation for the experimental conditions.

Table 9 Airborne microdroplets' mean diameters and standard deviations (in parenthesis).

Pressure (kPa)	275	415	550
With original nozzle (μm)	8.36 (3.3)	7.82 (3.1)	7.47 (2.8)
With rough nozzle (μm)	9.20 (4.0)	7.25 (2.3)	4.69 (1.6)
With smooth nozzle (μm)	11.42 (2.6)	9.31 (2.6)	7.60 (2.9)



(a)



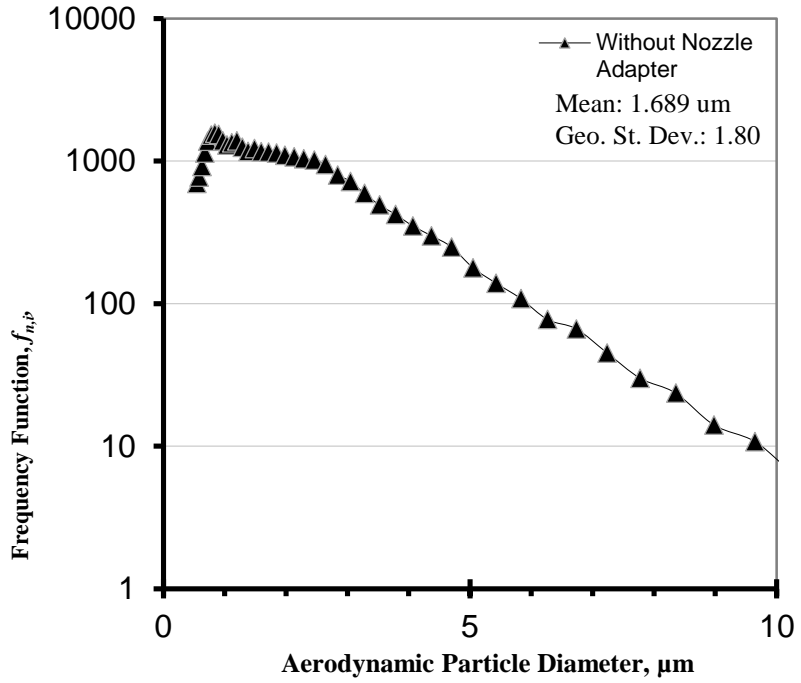
(b)

Figure 33 Effect of air pressure and nozzle surface on (a) airborne droplet diameters in MQL, and (b) their standard deviations.

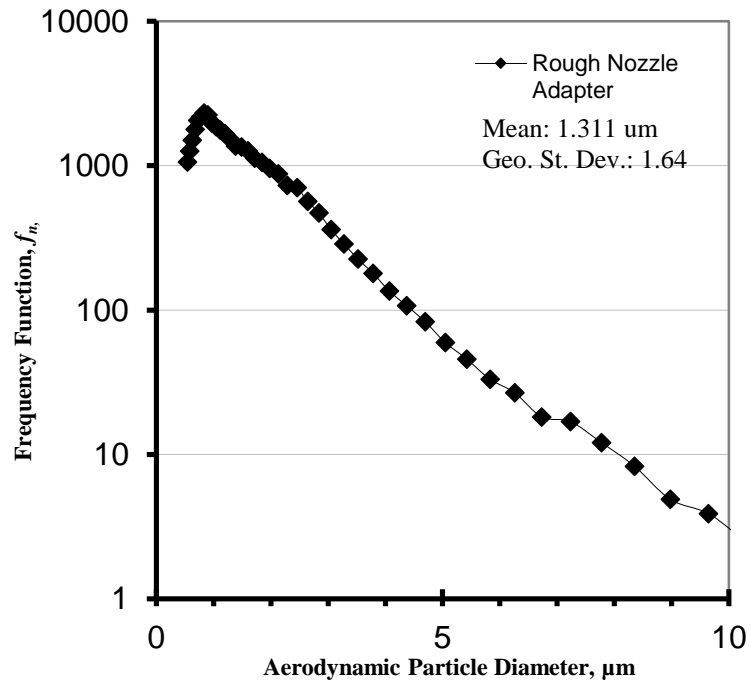
The quantitative results shown in Table 9 corroborate the observations made in Figure 28 about the decrease in size of the droplets with increase in air pressure and air speed. The largest decrease in droplet size was observed for the rough nozzle, where the mean droplet size decreased from 9.20 μm to 4.69 μm with the increase in pressure from 275 kPa to 550 kPa. This decrease in droplet size was coupled with increase in maximum air flow velocity from 11.2 m/s to 13.1 m/s. The smallest average droplet in this study is approximately 5 μm , produced with a rough nozzle at highest air pressure of 550 kPa. In contrast, the largest droplet is approximately 11 μm , generated with a smooth nozzle at lowest air pressure of 275 kPa. Table 9 and Fig. 33 summarize the experimental results. Higher pressures break oil into smaller droplets, the turbulence flow from the rough nozzle surface further contributes to even smaller mean aerodynamic diameters and more consistent size (smaller standard deviation). This relation between the droplet characteristics and the air pressure was also observed by Park et al. (2010). They observed a decrease in mean projected droplet diameter from 15.18 μm to 10.54 μm with the increase in pressure of compressed air from 27 kPa to 83 kPa when the distance between the nozzle and collecting substrate was kept constant at 50 mm.

The distribution plot for the MQL was also obtained using Aerodynamic Particle Sizer (APS 3321 TSI). The APS could only measure particles smaller than 20 μm in diameter due to its specifications. The trend observed using APS was same as that observed using the processing of images of droplets captured using Olympus STM 6 Microscope. Figure 34 shows that the mean of the droplets decreased from 1.689 μm to

1.311 μm when the rough nozzle adapter was used. The number of particles also increased with the use of as printed rough nozzle adapter as more droplets were being broken down into smaller droplets resulting in a larger particle count. The decrease in standard deviation from 1.80 for original nozzle to 1.64 for rough nozzle adapter showed that the size of the particles was more consistent with the use of rough nozzle adapter. The mean diameter measured using APS was lower than that determined using Olympus microscope (with 0.1 μm resolution) as particles around 1 μm in diameter could not be collected on the glass slide due to their small size. They either dispersed in air or evaporated as soon as they were deposited on the glass slide. The trends observed for data collected using the APS corroborated the fact that use of rough nozzle adapter decreased the aerodynamic diameter of the droplets. This observation was consistent with the data collected and analyzed using Olympus STM 6 Microscope and ImageJ. Dasch and Kurgin (2010) observed that for the dual channel MQL system, most mass for droplets was in 3-5 μm range, with only 11% of the droplets falling in submicron range. The experiments were conducted at a flowrate of 10 mL/h and the input pressure was not reported. Figure 34 shows that most of the droplets lie in the range of 1-2 μm . Dasch and Kurgin (2010) may have conducted experiments at a pressure lower than 550 kPa resulting in larger diameter of airborne droplets of Acculube LB6000 lubricant oil.



(a)



(b)

Figure 34 Droplet distribution generated using APS (a) without nozzle adapter (b) with rough nozzle adapter

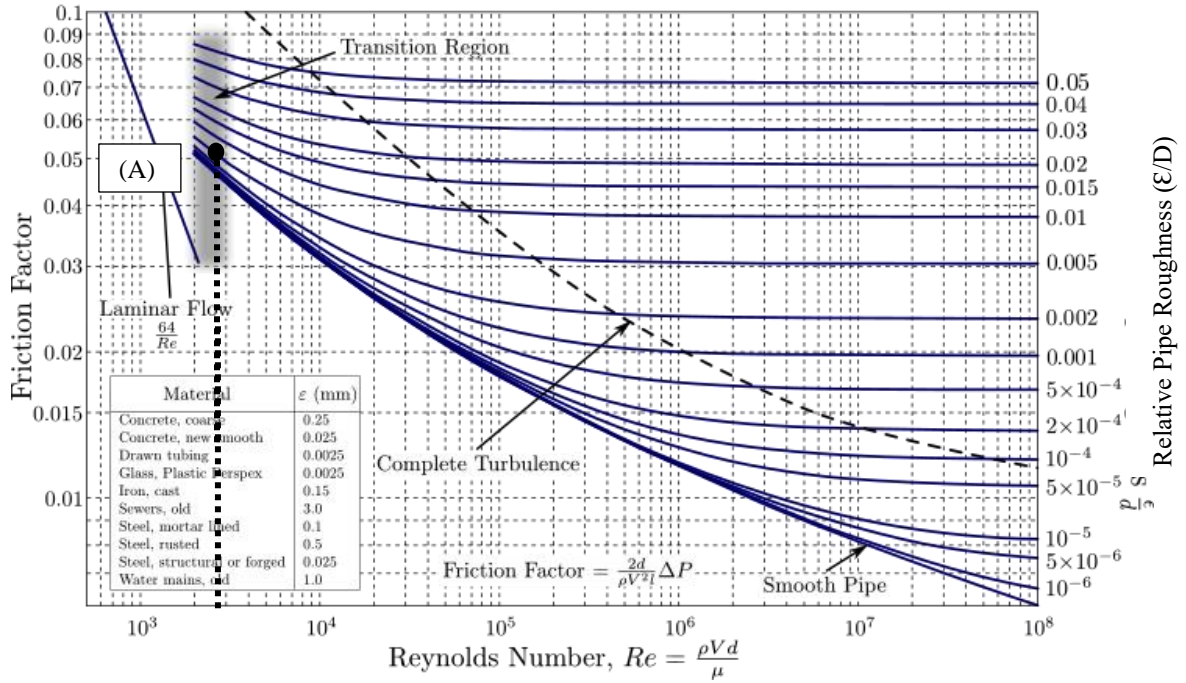


Figure 35 Moody Diagram (Reprinted from Beck and Collins, 2008)

The decrease in the droplet size can be explained by studying the Darcy-Weisbach equation (9) and the Moody chart (Fig 35).

$$\Delta P = f_d \frac{\rho V^2 L}{2 D} \quad (9)$$

Where

ΔP : Change in pressure (Pa)

f_d : Darcy-Weisbach friction factor (constant)

ρ : Density of the lubricant (kg/m^3)

V : Velocity of the lubricant (m/s)

L : Length of the internal channel of the adapter (m)

D : Diameter of the internal channel of the adapter (m)

\mathcal{E} : Surface roughness of adapter (mm)

Re : Reynolds number (constant)

μ : Dynamic viscosity (Pa.s)

The increase in surface roughness of the channel increases relative pipe roughness \mathcal{E}/D as the diameter of the channel remains constant. The Moody Diagram shows that the increase in relative pipe roughness (read from the right hand side of the diagram) leads to a higher friction factor for turbulent flow. The surface roughness of the rough nozzle adapter was 16.8 μm and 3.2 μm for the smooth nozzle adapter. The \mathcal{E}/D ratios were calculated to be 0.005 for the rough nozzle adapter and approximately 0.001 for the smooth nozzle adapter. Kinematic viscosity of Coolube 2210 EP was 18 mm^2/s . The values of flow velocity of lubricant (V), kinematic viscosity of lubricant (ν) and diameter of the nozzle (D) were plugged in equation (10) to calculate the Reynolds number.

$$Re = \frac{VD}{\nu} = \frac{13.2 \frac{m}{s} \times 0.0033 m}{1.8 \times 10^{-5} \frac{m^2}{s}} = 2420 \quad (10)$$

Where

Re : Reynolds number (constant)

V : Velocity of the lubricant measured using anemometer (m/s)

D : Diameter of the nozzle adapter (m)

ν : Kinematic viscosity of the lubricant (m^2/s)

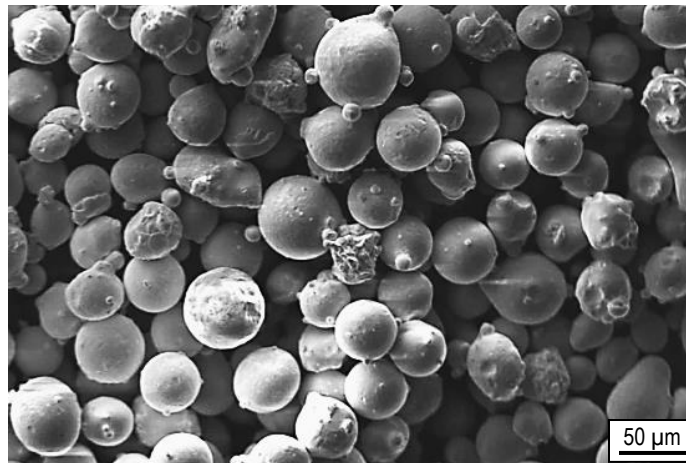
Since $Re= 2603$ and $\mathcal{E}/D= 0.005$ (point A on Figure 35), it suggests that the flow through the nozzle adapter was in turbulent flow regime. Assuming that the velocity of the lubricant is negligible in direction perpendicular to the air flow and the density remains constant, equation (9) shows that lower velocity will give a lower pressure drop ΔP across the flow channel. Lower drop in pressure due to rough surface led to smaller airborne diameter of droplets exiting through the rough nozzle.

The plots (Figs 30-32) generated for droplet distribution suggest that:

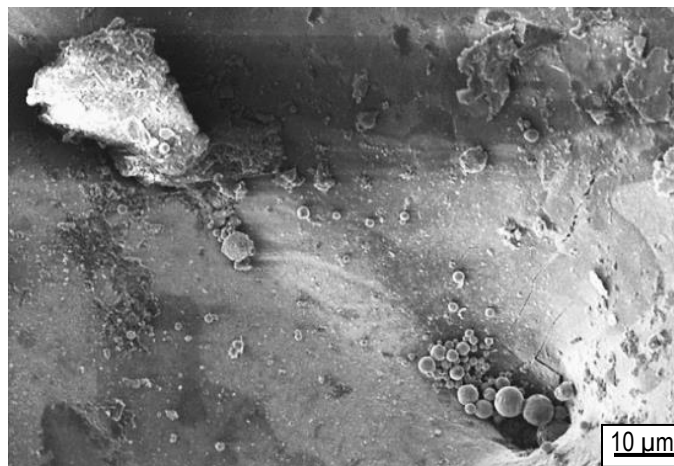
- The droplet diameters change drastically with pressure in a rough nozzle. At the highest pressure of 550 kPa coupled with higher pressure drop ΔP across the nozzle due to roughness, the smallest and most uniform droplet size can be obtained.
- The original nozzle is least affected by pressure change as it does not encounter the pressure drop ΔP due to surface roughness of the adapter.
- The smooth nozzle (polished ABS) and the original nozzle (extruded brass) produce similar droplet size with similar deviation at high pressure.

4.4 Micromilling of Inconel 718

The MQL results were applied to micromilling to study the effect of droplet size on machinability. Surface of as printed SLM'ed specimen is rough due to imperfect joining of adjacent layers, and defects due to phase transformation of metal powder by fast laser heating and fast cooling rate. Scanning electron microscopy examination shows many defects on as printed surface: depression cavities due to solidification shrinkage, partially melted powder particles, welded debris, micro cracks to name a few (Fig. 36).



(a)



(b)

Figure 36 Inconel 718 (a) in powder form, and (b) on xy-plane surface after SLM.

A precision component fabricated by SLM must be further processed to remove surface defects and achieve desirable final dimensions. The removal of the surface defects ensures proper functioning and prevents premature failure of the 3-D printed parts. Micromilling is one of the most versatile processes to shape a component while removing little material from a workpiece. Selecting micromilling for machinability study, therefore, is justified for the relatively expensive SLM'ed Inconel specimens.

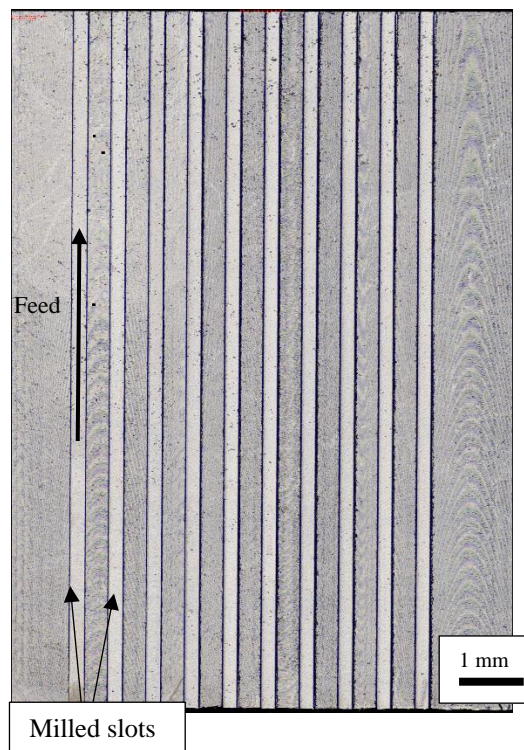
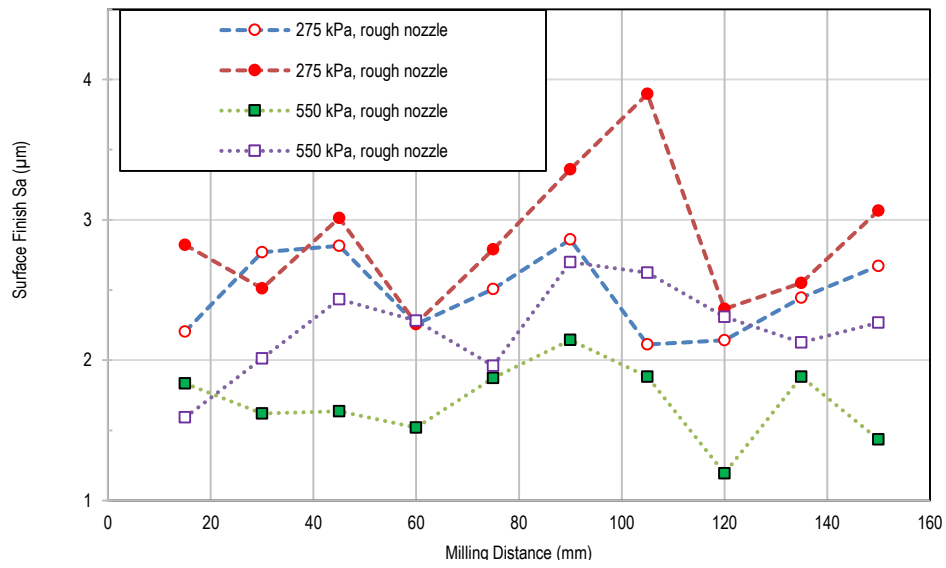


Figure 37 10 milled slots on Inconel 718

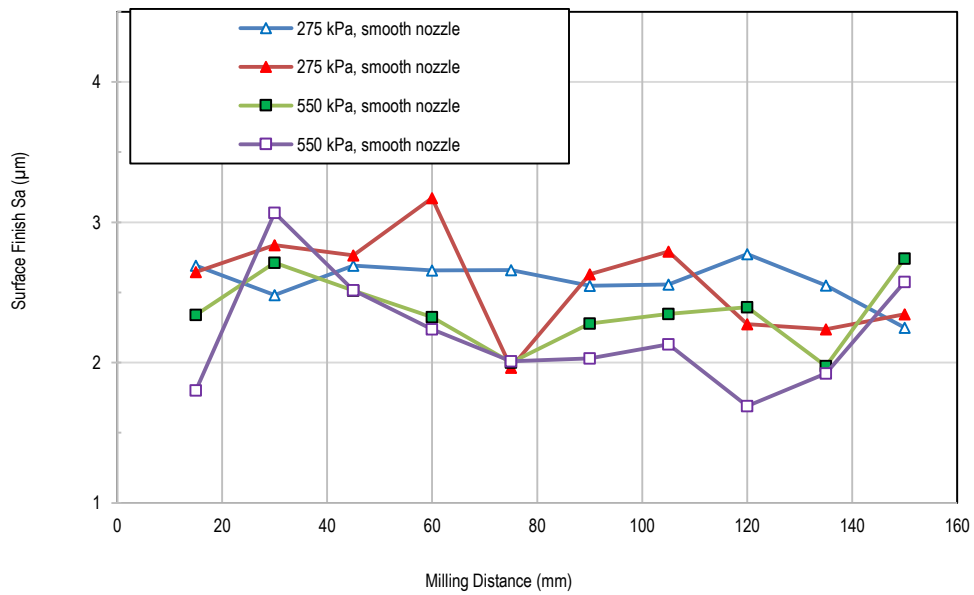
Both profile roughness R_a and surface roughness S_a were measured on micromilled slots. Although the profile roughness value was less than that of surface roughness, the data trends were somewhat similar in this study. Surface roughness S_a are presented in Fig. 39 as a function of cumulative milling distance. Surface finish is affected by tool wear, process parameters (speed, feed, depth of cut), lubricant

performance, machine and setup condition, and BUEs from “gummy” materials such as Inconel. By keeping the process parameters constant, we can assess the effectiveness of MQL when tool wear is insignificant, i.e. when a tool is machining at the beginning of a milling cut.

The high air pressure of 550 kPa and rough surface nozzle ($16.8 \mu\text{m } S_a$) produced approximately $5 \mu\text{m}$ lubricant droplets (Table 9). Such small droplets moving at high air velocity of 13.1 m/s under maximum air pressure effectively (i) removed the chips, (ii) lubricated the tool/workpiece interface, and (iii) reduced milled surface temperature. The resulting smooth surface finish of approximately $1.5 \mu\text{m } S_a$ was achieved favorably compared to approximately $2.5 \mu\text{m } S_a$ when MQL was operated at lower pressure of 275 kPa (Figs. 38a, 39b) and generated larger droplets at about $9 \mu\text{m}$ (Table 9). The effect was less pronounced when using MQL with smooth nozzle or lower pressure due to comparable droplets. Larger droplets had lesser MQL flow velocity (Figure 27) making it harder for them to remove chips and lubricate the tool/workpiece interface.

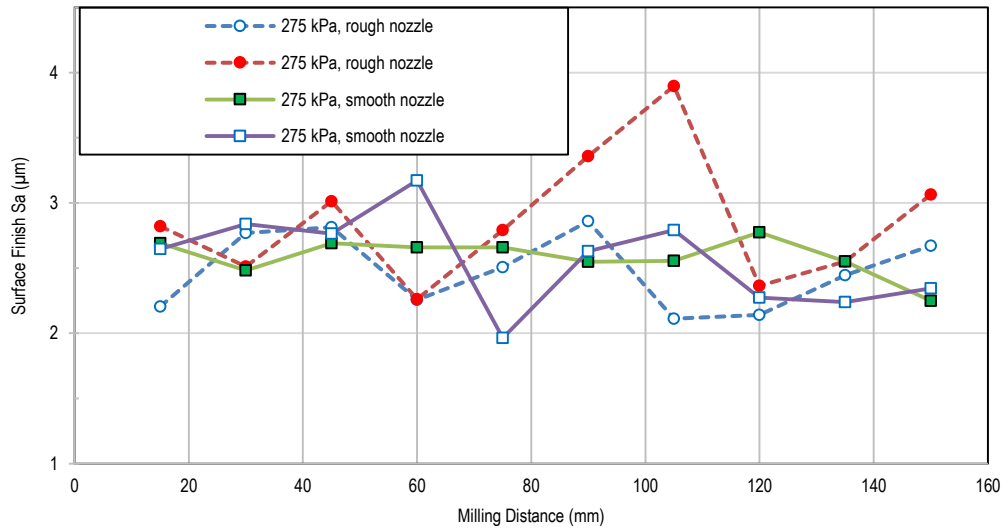


(a)

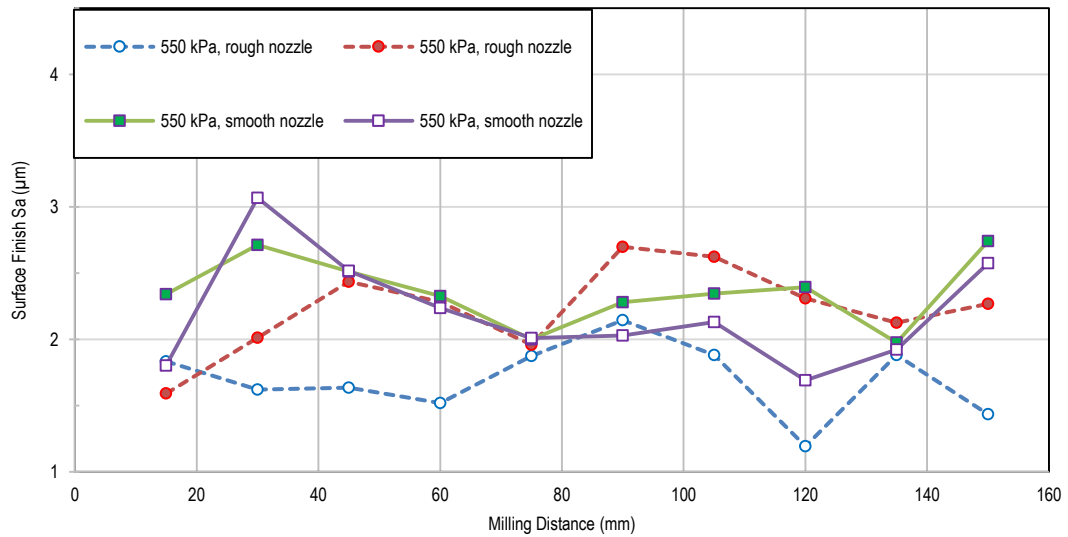


(b)

Figure 38 Area surface roughness when milling in MQL from a (a) rough nozzle, and (b) smooth nozzle.



(a)

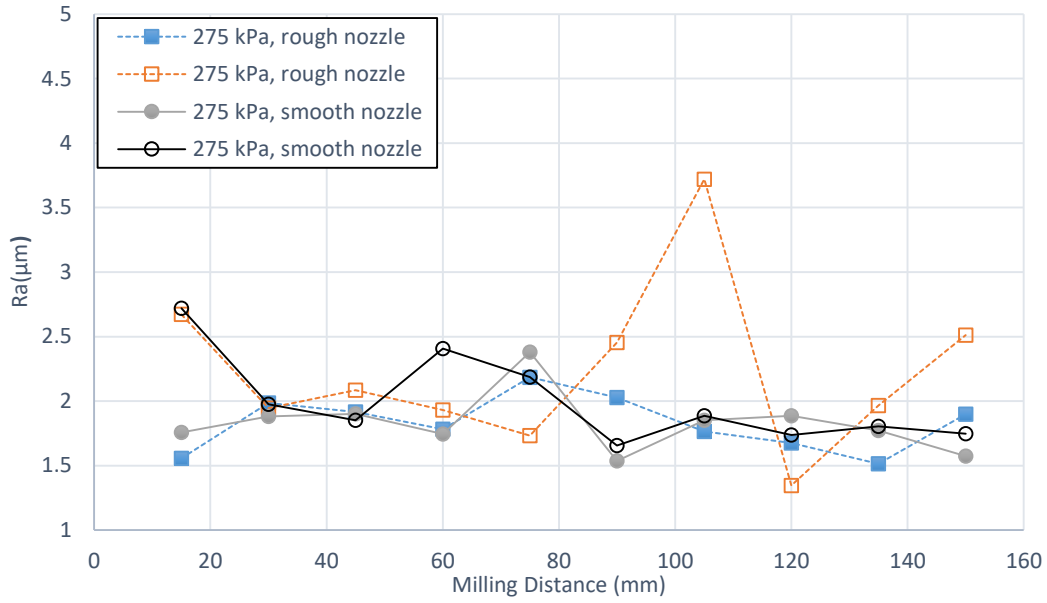


(b)

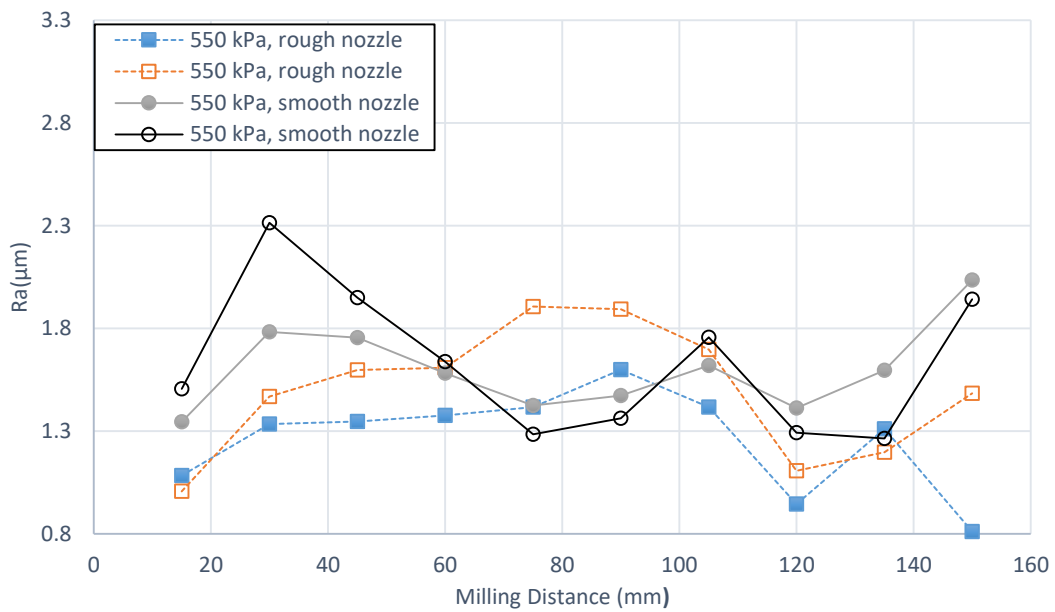
Figure 39 Area surface roughness when milling with air pressure of (a) 275 kPa and (b) 550 kPa.

Line roughness R_a (Figs. 40 and 41) followed a trend similar to the surface roughness (S_a) though its values were lesser than those measured for surface roughness. The reason for this aberration was the number of data points and regions considered for measurement. Profile roughness measured along the center profile of the slot while the surface roughness accounted for all the data points within a $150\ \mu\text{m} \times 500\ \mu\text{m}$ rectangle at the center of the slot.

The trend for line roughness measured at 275 kPa for workpieces machined using rough and smooth nozzle was not very clear due to their comparable sizes. The mean airborne droplet diameter was $9.20\ \mu\text{m}$ for rough nozzle and $11.42\ \mu\text{m}$ for smooth nozzle at 275 kPa. It became clearer at 550 kPa as the droplets generated at this pressure through the rough nozzle were smaller (approximately $5\ \mu\text{m}$) than those generated through the smooth nozzle ($7.6\ \mu\text{m}$). Droplets generated at 550 kPa using a rough nozzle were travelling at a high air velocity of 13.1 m/s. This helped the droplets to effectively lubricate the workpiece/tool interface and blow away the chips ensuring a R_a of approximately $1.9\ \mu\text{m}$ (Fig 41b). Similar trends were observed for R_a and S_a , though the minimum value of S_a measured was approximately $1.5\ \mu\text{m}$ compared to $0.8\ \mu\text{m}$ of R_a . Figure 41 shows that increasing pressure decreased the resulting profile finish due to better lubrication by smaller droplets generated at high pressure.

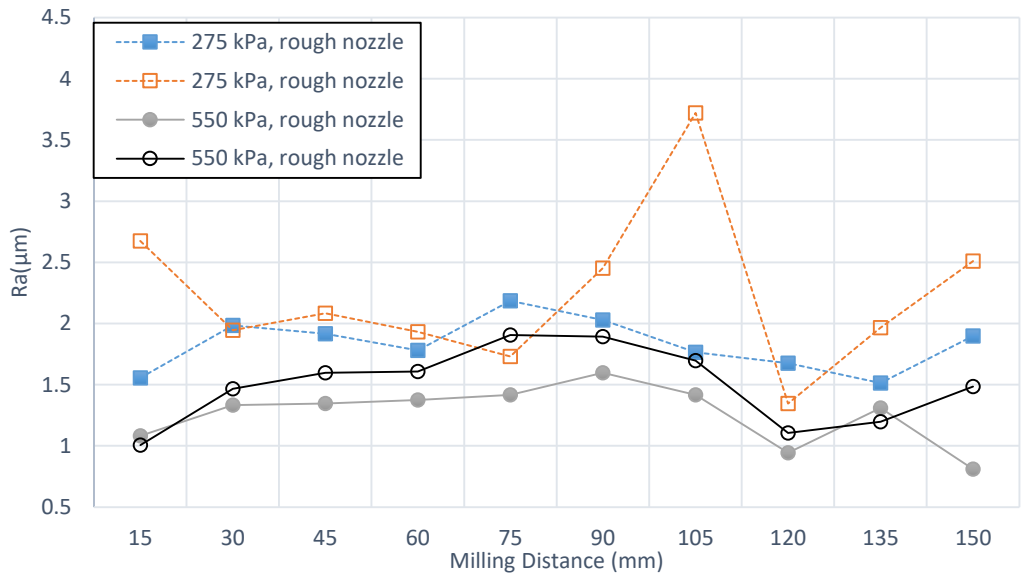


(a)

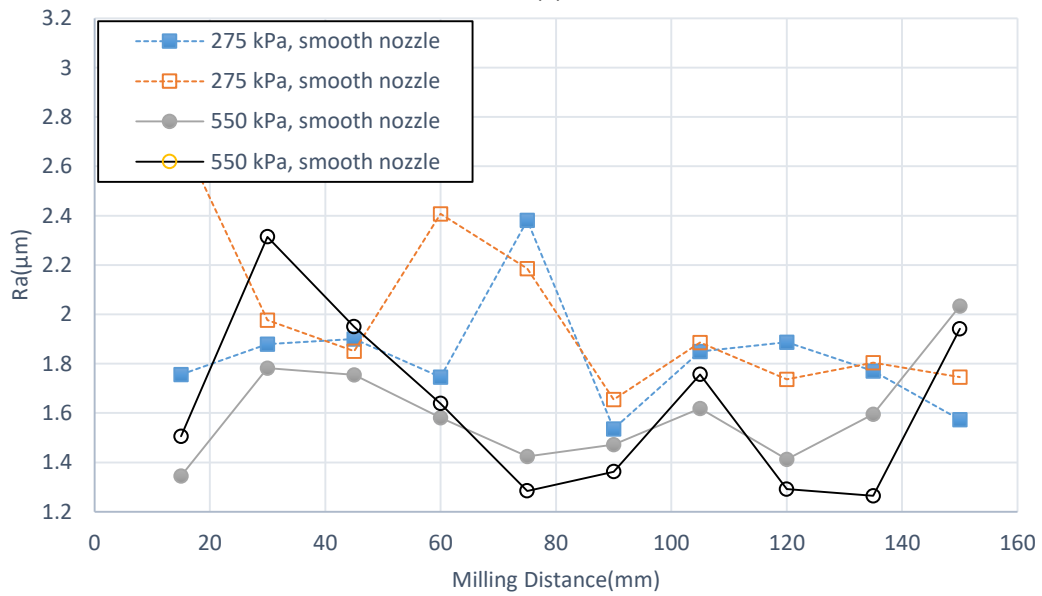


(b)

Figure 40 Profile roughness when milling with air pressure of (a) 275 kPa and (b) 550 kPa.



(a)

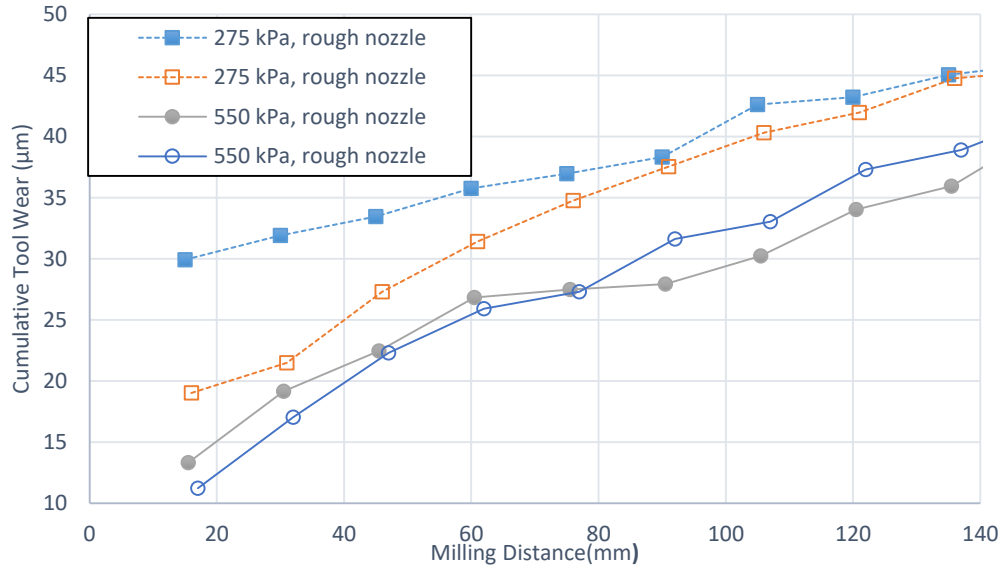


(b)

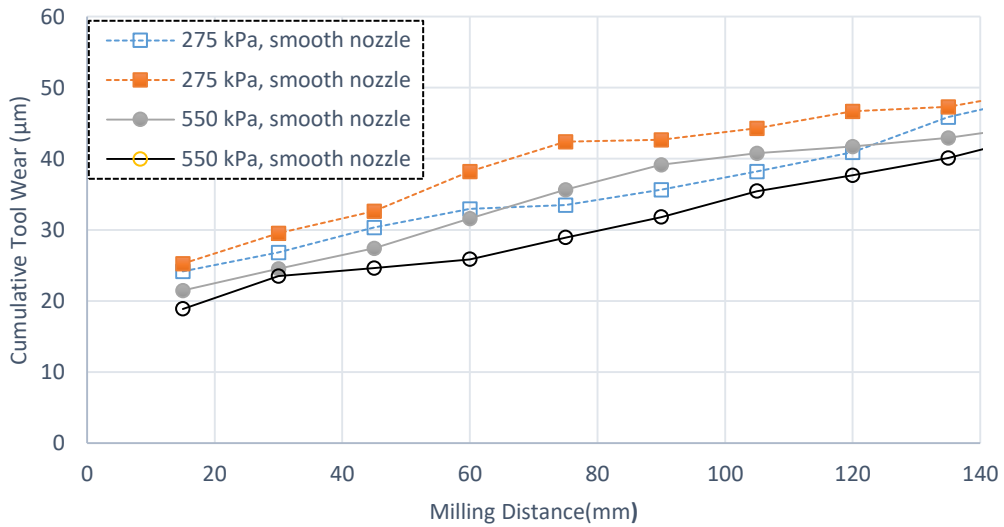
Figure 41 Profile roughness when milling in MQL from a (a) rough nozzle, and (b) smooth nozzle.

Post processing, such as finish machining, of SLM'ed metals is necessary for critical engineering components since finish machining drastically reduces the area surface roughness S_a from 17 μm to approximately 1.5 μm . A polishing technique is required if a surface finish in submicron range is needed.

Figure 42 compares the changes of the slot widths (tool wear) as the function of cumulative milling distance. This slot width change was contributed solely by the tool flank wear on both flutes of a micromilling tool. The rough nozzle, operating at 550 kPa, produced the smallest droplets of $\sim 5 \mu\text{m}$. Such small droplets, when flying at high speed of 13.5 m/s (Fig. 25) due to strong air pressure, effectively lubricated the tool and reduced its temperature. This resulted in lowest tool wear –in both magnitude and slope– as shown in Fig. 42a. The total tool wear for this configuration was approximately 41 μm . The high pressure on smooth nozzle, generated slightly larger droplets of $\sim 7 \mu\text{m}$, seemed to have a lesser effect on tool wear (Fig. 42b). At the lower pressure of 275 kPa a rough nozzle produced $\sim 9 \mu\text{m}$ droplets compared to $\sim 11 \mu\text{m}$ droplets from the smooth nozzle (Table 9); however the low droplet density at 275 kPa did not provide adequate lubrication to tool and workpiece. This might be the cause for unexpected tool wear of approximately 49 μm when using with MQL at low air pressure along with smooth nozzle. Another issue was the difficulty and inaccuracy of slot width data when measuring slot width machined with excessive tool wear as evidence from the significant amount of burr along the slot walls (Fig. 43).



(a)



(b)

Figure 42 . Cumulative tool wear when milling in MQL from (a) rough nozzle, and (b) smooth nozzle

Table 10 Total tool wear (slot width change, μm)

	Input Air Pressure	Input Air Pressure
	275 kPa	550 kPa
Rough Nozzle	45.98	40.62
	45.43	41.93
Smooth Nozzle	48.92	44.84
	49.72	43.51

Limited published data were found on the effect of MQL air pressure on machinability. The reduction in tool wear was shown in this study when increasing air pressure and air flow velocity, therefore producing consistent and small droplet sizes for effective lubrication. Obikawa et al. (2006) published similar trend when study machining steel in MQL. Grooving 0.45% carbon steel using TiC/TiCN/TiN coated carbide tool at cutting speeds of 4 and 5 m/s, the authors observed that corner wear of the tool decreased from ~0.13 mm to ~0.07 mm when the air pressure was increased from 300 kPa to 700 kPa. They attributed this decrease in wear to cooling effect of the high speed of compressed air. They suggested that the air cooled due to rapid expansion on its exit from the nozzle cooling down the tool and workpiece. They corroborated this theory by measuring the temperature of air at the exit of nozzle and concluded that the temperature of exiting air was 20°K less than that of ambient air. Kamata (2007) performed finish turning of IN 718 in MQL. Changing air pressure from 300 to 700 kPa decreased the corner tool wear

from 0.13 mm to 0.07 mm for TiCN/Al₂O₃/TiN and TiN/AlN but the tool wear were not better than that from dry machining.

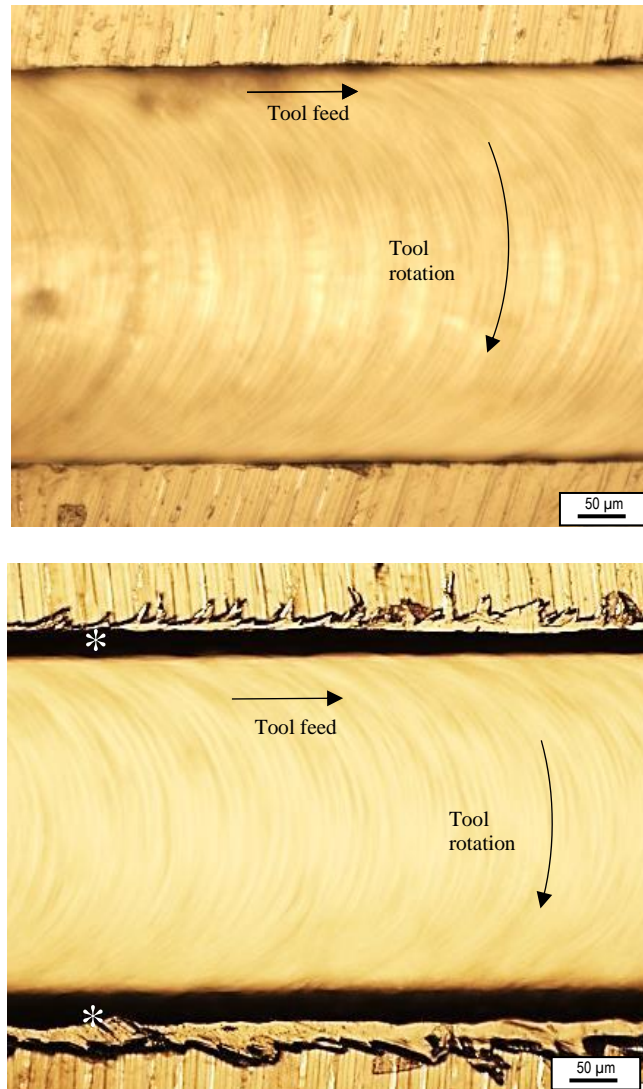


Figure 43 Insignificant burr at cumulative milling distance of 5 mm, but lots of burr (label *) are formed after 135 mm milling distance. Note the narrower slot width of the latter

5. CONCLUSIONS AND RECOMMENDATIONS

Simulation of through-tool minimum quantity lubrication (MQL) was performed by mimicking geometry of a twist drill with internal cooling channels. Droplet sizes and their effects on micromilling of Inconel 718 were investigated. This study showed:

- 1) Both air pressure and surface roughness of MQL nozzle affect the lubricant droplet sizes. The smallest diameter airborne droplet of $\sim 5 \mu\text{m}$ was achieved.
- 2) MQL droplets generated at 550 kPa using a polished nozzle adapter had a higher air flow velocity of 14.2 m/s when compared to 13.1 m/s generated using the rough nozzle adapter.
- 3) The $5 \mu\text{m}$ droplets under high air pressure effectively reduces tool wear while improving surface finish of micromilled Inconel produced by selective laser melting (SLM).
- 4) The rough surface of $\sim 17 \mu\text{m}$ S_a after SLM was significantly reduced to $\sim 1.5 \mu\text{m}$ S_a after micromilling.
- 5) At 550 kPa, the R_a using rough nozzle was approximately $1 \mu\text{m}$ compared approximately $1.5 \mu\text{m}$ obtained using smooth nozzle.

Future works should include:

- a) Study of different tool coatings when micromilling SLM'ed Inconel under MQL.
- b) Simulate the turbulence flow of micromist inside a rough or smooth channel.
- c) Measure/simulate air flow in the neighbourhood of exit end of a smooth or rough nozzle.
- d) Study the effects of pressure and air speed when using actual through-tool MQL.

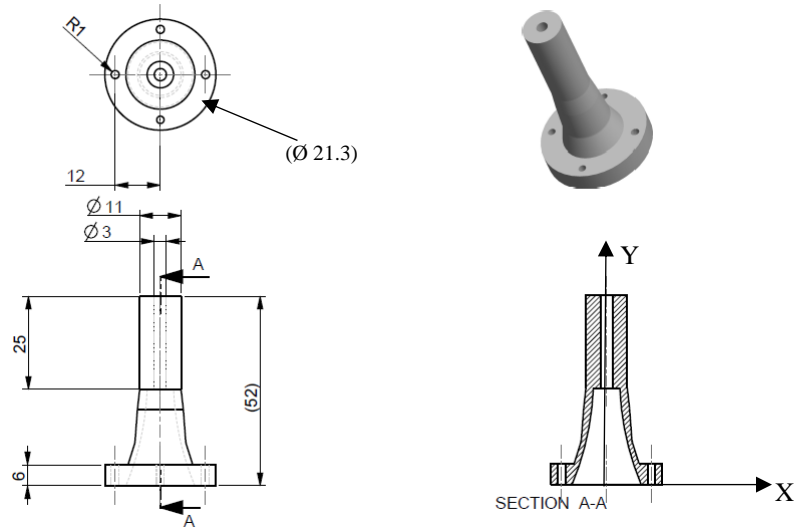
REFERENCES

- Alicona InfiniteFocus Microscope (n.d.), Retrieved from:
<http://www.alicon.com/products/infinitefocus>
- Beck, S; Collins, R. (2008) Moody Diagram, University of Sheffield. Retrieved from
https://commons.wikimedia.org/wiki/File:Moody_diagram.jpg
- Berestovskyi, D.(2013) Surface finish modelling in micromilling of biocompatible materials, Thesis, Texas A&M University Libraries
- Dasch, J.M.; Kurgin, S.K. (2010) A characterization of mist generated from minimum quantity lubrication (MQL) compared to wet machining, *Int. J. Machining and Machinability of Materials*, Vol. 7, (1-2): 82–95.
- Dwuletzi, H. (2015) Minimum Quantity Lubrication vs Traditional Flood Application, 5th International Conference on Metal Removal Fluids.
- Hinds, W.C. (1999) *Aerosol Technology; Properties, Behavior and Measurement of Airborne Particles*, 2nd Edition, (1999), New York, John Wiley and Sons Inc.
- Kamata, Y. ; Obikawa, T. (2007) High speed MQL finish-turning of Inconel 718 with different coated tools, *Journal of Materials Processing Technology*, 192–193: 281–286.
- Kaynak, Y., (2014) Evaluation of machining performance in cryogenic machining of Inconel 718 and comparison with dry and MQL machining, *Int J Adv Manuf Technol*, 72: 919–933.

- Li, Q.; Krell, J.; Lerma, I.; Alvaradao, J.; Edinbarough, I; Hung, W. (2015) Characterization of micro mist for effective machining, ASME International Engineering Congress and Exposition, Houston, Nov 16-19, IMECE 2015-53632.
- Obikawa, T.; Kamata, Y.; Asano, Y.; Nakayama, K.; Otieno, A. W. (2008) Micro-liter lubrication machining of Inconel 718, International Journal of Machine Tools & Manufacture, 48: 1605–1612.
- Obikawa, T.; Kamataa, Y.; Shinozukab, J. (2006) High-speed grooving with applying MQL. International Journal of Machine Tools & Manufacture, 46: 1854–1861.
- Olympus STM 6 (n.d.), Retrieved from: http://www.used-line.com/pictures/10/9809310_1.jpg
- Park, K.H.; Yume, J.O.; Yoon, M.; Kwon, P. (2010) A study on droplets and their distribution for minimum quantity lubrication (MQL), Int. J. of Machine Tools and Manufacture, 50: pp. 824-833.
- Performance Microtools (2018). Retrieved from: <http://www.pmtnow.com/end-mill/TR>
- Sai, S. S.; ManojKumar K.; Ghosh, A. (2015) Assessment of spray quality from an external mix nozzle and its impact on SQL grinding performance, International Journal of Machine Tools & Manufacture, 89: 132–141
- Sakaida, A.; Toshihisa, T.; Takada, K.; Takeda, K. (2006) Micro-mist generation method and apparatus, US 7131603 B2.

- Tai, B. L.; Dasch, J.M.; Shih, A. J (2011) Evaluation and comparison of lubricant properties in minimum quantity lubrication machining, *Machining Science and Technology*, 15(4): 376-391.
- Tai, B. L.; Stephenson, D. A.; Furness, R. J.; Shih, A. J. (2014) Minimum Quantity Lubrication (MQL) in Automotive Powertrain Machining, *Procedia CIRP*, vol. 14; pp. 523-528.
- Uzun, I.; Aslantas, K.; Bedir, F. (2013) An experimental investigation of the effect of coating material on tool wear in micro milling of Inconel 718 super alloy, *Wear* 300: 8–19.
- Uzun, I.; Aslantas, K.; Bedir, F.(2014) The effect of minimum quantity lubrication and cryogenic pre-cooling on cutting performance in micro-milling on Inconel 718, *Institution of Mechanical Engineers Part B, Journal of Engineering Manufacture*, 229(12): 1-10.
- Unist Coolubricator (n.d.) Retrieved: <http://unist.com/pdf/coolubricator.pdf>
- Wang, Z.; Kovvuria, V.; Araujo, A.; Bacci, M.; Hung, N.P.; Bukkapatnam S.T.S. (2016) Built-up-edge Effects on Surface Deterioration in Micromilling Processes, *Journal of Manufacturing Processes*, 24; 321–327.
- Zhang, S.; Li, J.F.; Wang, Y. (2012) Tool life and cutting forces in end milling Inconel 718 under dry and minimum quantity cooling lubrication cutting conditions, *Journal of Cleaner Production*, *Journal of Cleaner Production*, 32; 81-87.

APPENDIX A
DESIGN OF NOZZLE ADAPTER



Section	Y(mm)	X (mm)	
		Outside Radius	Inside Radius
1	0	10.65	9.40
2	11.75	6.90	5.60
3	20.75	6.25	5.00
4	26.25	5.55	3.60

Figure 44 Design of Nozzle Adapter

Unit	mm
Material	ABS Plastic
Scale	1 : 2

Note:
OD and ID of sections 1-4 are blended using the “Blend” tool in Pro Engineer

APPENDIX B EQUIPMENT

B.1 UNIST MQL Dispensing Unit

UNIST MQL Coolubricator system was used to generate the mist. These positive displacement systems are self-contained systems ensuring continuous fluid delivery. It operates using an adjustable pulse generator, an air metering screw and stroke metering pump. The stroke length and frequency of the pulse generator can be changed to adjust the lubricant output. The number of cycles of piston can be adjusted between 2 to 200 cycles per minute. Output of liquid is adjusted using the brass knob on the metering screw. An air metering screw is used to adjust the flow of compressed air that atomizes the air. The coolant reservoir has a capacity of 10 ounces, which equals to 9000 drops of coolant. The flexible nozzle of the units is used to deliver the lubricant to the targeted area.



Figure 45 UNIST MQL Lubrication System (Reprinted from “Unist Coolubricator”, n.d.)

B.2 Olympus STM 6 Optical Microscope

The microscope was used to take images of the droplets deposited on the glass slides. These images were used to extract the data about the area covered by the droplets, projected diameter of the droplets and contact angles. DP 70 12.5 MP camera was used in the microscope to take and save pictures. The images were then imported for ImageJ software for further analysis. The microscope had the resolution of 0.1 μm . The microscope had 4 objective lenses installed. 1.25x, 5x and 10x objective lenses were used to capture images. The worktable can be moved in X and Y directions and the camera could be moved in Z direction. The Z direction can be used in coarse and fine mode to get a focused image.



Figure 46 Olympus STM 6 Microscope (Reprinted from "Olympus STM 6", n.d.)

B.3 HAAS OM2 CNC Milling Machine

HAAS OM2 CNC milling machine was used to run the milling experiments. The machine used an air bearing spindle which allowed the machine to have a maximum spindle speed of 50,000 rpm. The machine had three degrees of freedom, which were sufficient to perform the machining experiments.

Table 11 HAAS OM2 CNC Milling Machine Technical Specifications (Reprinted from Berestovskyi, 2013)

Travels	S.A.E.	Metric
X axis	12''	305 mm
Y axis	10''	254 mm
Z axis	12''	305 mm
Table	S.A.E.	Metric
Length	20''	508 mm
Width	10''	254 mm
Max weight on table	150 lb	68 kg
Spindle	S.A.E.	Metric
Taper	ISO/20	ISO/20
MAX speed	50000 rpm	50000 rpm
MIN speed	1000 rpm	1000 rpm
Feed rates	S.A.E.	Metric
Rapids on X, Y, and Z	757 in/min	19.2 m/min
MAX cutting	500 in/min	12.7 m/min
Accuracy	S.A.E.	Metric
Positioning	-	±0.005 mm
Repeatability	-	±0.003 mm
General	S.A.E.	Metric
Air required	1 scfm, 40-70 psi	28 L/min, 2.8-4.8 bar
Machine weight	1500 lb	680

B.4 Alicona InfiniteFocus Microscope

The electronic microscope was used to measure the profile and surface roughness of the milled slots. The microscope used only one multi-functional measurement sensor to extract measurements for all relevant surface features. Microscope used 5X, 10X and

20X objective lens to take the images of the workpiece which were then post processed in the software suite to generate slot width, profile roughness and surface roughness.



Figure 47 Alicona InfiniteFocus Microscope (Reprinted from "Alicona InfiniteFocus", n.d.)

Table 12 Technical specifications of Alicona InfiniteFocus Microscope (Reprinted from "Alicona InfiniteFocus", n.d.)

Measurement principle	non-contact, optical, three-dimensional, based on Focus-Variation								
Positioning volume (X x Y x Z)	100 mm x 100 mm x 100 mm = 1000000 mm ³ (optional: 200 mm x 200 mm x 100 mm = 4000000 mm ³)								
Objective magnification		2.5x	5x	10x	10x	20x	20x	50x	100x
				HX		HX			
Working distance	mm	8.8	23.5	37	17.5	30	19	11	4.5
Lateral measurement range (X,Y) (X x Y)	mm	5.63	2.82	1.62	1.62	0.7	0.81	0.32	0.16
	mm ²	31.7	7.85	2.62	2.62	0.49	0.66	0.10	0.03
Vertical resolution	nm	2300	410	250	100	80	50	20	10

Height step accuracy (1 mm)	%	n.a.	0.05	0.05	0.05	0.05	0.05	0.05	0.05
Max. measurable area	mm ²	10000	10000	10000	10000	10000	10000	3965	990
	mm ²	40000	40000	40000	40000	24780	24780	3965	990
Optional									
Min. measurable roughness (Ra)	μm	7	1.2	0.75	0.3	0.24	0.15	0.06	0.03
Min. measurable roughness (Sa)	μm	3.5	0.6	0.375	0.15	0.12	0.075	0.03	0.015
Min. measurable radius	μm	20	10	5	5	3	3	2	1

APPENDIX C
NC CODE FOR SLOT MILLING

Code used to micromill slots on 3D printed Inconel

%
O48908 (WALEED_THESIS)
N35 G00 G17 G40 G90
(STANDARD START-UP SETTINGS)

N40 G21
(MILLIMETERS)

N45 T1
(IDENTIFIES TOOLING)

N55 G43 H01
(CALLS OUT TOOL LENGTH COMPENSATION)

N50 G90 G54 G01 G94 F600. X-0.125 Y-0.125 Z5.0 (Feed rate in mm/min)
N55 G01 F20. Z1.0
(MOVES MACHINE TO X Y POSITION AND ZOFFSET 5)
(COORDINATES SET IN LINE G54 IN OFFSETS)

N70 M97 P11111 L10
(M97 CALLS FOR SUB-ROUTINE)
(P11111 --> SUBROUTINE AT LINE N11111)
(L1 --> NUMBER OF TIMES TO REPEAT SUBROUTINE)

N75 M00
(HARD STOP)

N80 M30

(CONDITION 1)
N11111 S17041 M03
N11112 X0.5 Y-1. Z1.
N11114 G91 G01 Z-0.02 F40. (DOC 20 MICRONMETER)
N11115 Y15.5
N11116 F444. Z3.
N11117 G01 X0.5 Y-14.5 Z3.
N11118 M99
%

APPENDIX D
NC CODE FOR AIR SPEED

%
O01122
N35 G00 G17 G40 G90
(Standard START-UP Settings)
N40 G21
(Metric coordinate positioning, setting 9 = mm)
N45 G90 G59 G00 X0. Y0.
G01 X+2.5 Y+25. F1000
(Work OFFset Positioning Coordinate #1)
(topleft point of measurement way, 5x5 mm)
N50 M97 P11111 L18
(P1111: Subroutine in line N11111, 18 reps)
N55 M30
(Ends Programm)
N11111 G91
N11112 G04 P5000
N11113 G01 Y-5.0
N11114 G04 P5000
N11115 G01 Y-5.0
N11116 G04 P5000
N11117 G01 Y-5.0
N11118 G04 P5000
N11119 G01 Y-5.0
N11120 G04 P5000
N11121 G01 Y-5.0
N11122 G04 P5000
N11123 G01 Y-5.0
N11124 G04 P5000
N11125 G01 Y-5.0
N11126 G04 P5000
N11127 G01 Y-5.0
N11128 G04 P5000
N11129 G01 Y-5.0
N11130 G04 P5000
N11131 G01 Y-5.0
N11132 G04 P5000
N11133 G01 Y+50.0 X+5.0
N11134 M99